



UNIVERSITY OF LEEDS

This is a repository copy of *A comprehensive quantification of global nitrous oxide sources and sinks*.

White Rose Research Online URL for this paper:
<http://eprints.whiterose.ac.uk/166534/>

Version: Accepted Version

Article:

Tian, H, Xu, R, Canadell, JG et al. (54 more authors) (2020) A comprehensive quantification of global nitrous oxide sources and sinks. *Nature*, 586 (7828). pp. 248-256. ISSN 0028-0836

<https://doi.org/10.1038/s41586-020-2780-0>

© The Author(s), under exclusive licence to Springer Nature Limited 2020. This is an author produced version of an article published in *Nature*. Uploaded in accordance with the publisher's self-archiving policy.

Reuse

Items deposited in White Rose Research Online are protected by copyright, with all rights reserved unless indicated otherwise. They may be downloaded and/or printed for private study, or other acts as permitted by national copyright laws. The publisher or other rights holders may allow further reproduction and re-use of the full text version. This is indicated by the licence information on the White Rose Research Online record for the item.

Takedown

If you consider content in White Rose Research Online to be in breach of UK law, please notify us by emailing eprints@whiterose.ac.uk including the URL of the record and the reason for the withdrawal request.



eprints@whiterose.ac.uk
<https://eprints.whiterose.ac.uk/>

A comprehensive quantification of global nitrous oxide sources and sinks

Hanqin Tian¹, Rongting Xu¹, Josep G. Canadell², Rona L. Thompson³, Wilfried Winiwarter^{4,5}, Parvatha Suntharalingam⁶, Eric A. Davidson⁷, Philippe Ciais⁸, Robert B. Jackson^{9,10,11}, Greet Janssens-Maenhout^{12,13}, Michael J. Prather¹⁴, Pierre Regnier¹⁵, Naiqing Pan^{1,16}, Shufen Pan¹, Glen P. Peters¹⁷, Hao Shi¹, Francesco N. Tubiello¹⁸, Sönke Zaehle¹⁹, Feng Zhou²⁰, Almut Arneht²¹, Gianna Battaglia²², Sarah Berthet²³, Laurent Bopp²⁴, Alexander F. Bouwman^{25,26,27}, Erik T. Buitenhuis^{6,28}, Jinfeng Chang^{8,29}, Martyn P. Chipperfield^{30,31}, Shree R. S. Dangal³², Edward Dlugokencky³³, James W. Elkins³³, Bradley D. Eyre³⁴, Bojie Fu^{16,35}, Bradley Hall³³, Akihiko Ito³⁶, Fortunat Joos²², Paul B. Krummel³⁷, Angela Landolfi^{38,39}, Goulven G. Laruelle¹⁵, Ronny Lauerwald^{8,15,40}, Wei Li^{8,41}, Sebastian Lienert²², Taylor Maavara⁴², Michael MacLeod⁴³, Dylan B. Millet⁴⁴, Stefan Olin⁴⁵, Prabir K. Patra^{46,47}, Ronald G. Prinn⁴⁸, Peter A. Raymond⁴², Daniel J. Ruiz¹⁴, Guido R. van der Werf⁴⁹, Nicolas Vuichard⁸, Junjie Wang²⁷, Ray F. Weiss⁵⁰, Kelley C. Wells⁴⁴, Chris Wilson^{30,31}, Jia Yang⁵¹ & Yuanzhi Yao¹

¹International Center for Climate and Global Change Research, School of Forestry and Wildlife Sciences, Auburn University, Auburn, AL, USA

²Global Carbon Project, CSIRO Oceans and Atmosphere, Canberra, Australian Capital Territory, Australia

³Norsk Institutt for Luftforskning, NILU, Kjeller, Norway

⁴International Institute for Applied Systems Analysis, Laxenburg, Austria

⁵Institute of Environmental Engineering, University of Zielona Góra, Zielona Góra, Poland.

⁶School of Environmental Sciences, University of East Anglia, Norwich, UK

⁷Appalachian Laboratory, University of Maryland Center for Environmental Science, Frostburg, MD, USA

⁸Laboratoire des Sciences du Climat et de l'Environnement, LSCE, CEA CNRS, UVSQ UPSACLAY, Gif sur Yvette, France

⁹Department of Earth System Science, Stanford University, Stanford, CA, USA

¹⁰Woods Institute for the Environment, Stanford University, Stanford, CA, USA

¹¹Precourt Institute for Energy, Stanford University, Stanford, CA, USA

¹²European Commission, Joint Research Centre (JRC), Ispra, Italy

¹³Ghent University, Faculty of Engineering and Architecture, Ghent, Belgium

¹⁴Department of Earth System Science, University of California Irvine, Irvine, CA, USA

¹⁵Department Geoscience, Environment & Society, Université Libre de Bruxelles, Brussels, Belgium

¹⁶State Key Laboratory of Urban and Regional Ecology, Research Center for Eco-Environmental Sciences, Chinese Academy of Sciences, Beijing, China

¹⁷CICERO Center for International Climate Research, Oslo, Norway

¹⁸Statistics Division, Food and Agriculture Organization of the United Nations, Via Terme di Caracalla, Rome, Italy

¹⁹Max Planck Institute for Biogeochemistry, Jena, Germany

²⁰Sino-France Institute of Earth Systems Science, Laboratory for Earth Surface Processes, College of Urban and Environmental Sciences, Peking University, Beijing, China

²¹Karlsruhe Institute of Technology, Institute of Meteorology and Climate Research/Atmospheric Environmental Research, Garmisch-Partenkirchen, Germany

46 ²²Climate and Environmental Physics, Physics Institute and Oeschger Centre for Climate Change
47 Research, University of Bern, Bern, Switzerland
48 ²³Centre National de Recherches Météorologiques (CNRM), Université de Toulouse, Météo-
49 France, CNRS, Toulouse, France
50 ²⁴LMD-IPSL, Ecole Normale Supérieure / PSL Université, CNRS; Ecole Polytechnique,
51 Sorbonne Université, Paris, France
52 ²⁵PBL Netherlands Environmental Assessment Agency, The Hague, The Netherlands
53 ²⁶Department of Earth Sciences – Geochemistry, Faculty of Geosciences, Utrecht University,
54 Utrecht, The Netherlands
55 ²⁷Key Laboratory of Marine Chemistry Theory and Technology, Ministry of Education, Ocean
56 University of China, Qingdao, China
57 ²⁸Tyndall Centre for Climate Change Research, School of Environmental Sciences, University of
58 East Anglia, Norwich, UK
59 ²⁹College of Environmental and Resource Sciences, Zhejiang University, Hangzhou, China.
60 ³⁰National Centre for Earth Observation, University of Leeds, Leeds, UK
61 ³¹Institute for Climate and Atmospheric Science, School of Earth and Environment, University of
62 Leeds, Leeds, UK
63 ³²Woods Hole Research Center, Falmouth, MA, USA
64 ³³NOAA Global Monitoring Laboratory, Boulder, CO, USA
65 ³⁴Centre for Coastal Biogeochemistry, School of Environment Science and Engineering,
66 Southern Cross University, Lismore, New South Wales, Australia
67 ³⁵Faculty of Geographical Science, Beijing Normal University, Beijing, China
68 ³⁶Center for Global Environmental Research, National Institute for Environmental Studies,
69 Tsukuba, Japan
70 ³⁷Climate Science Centre, CSIRO Oceans and Atmosphere, Aspendale, Victoria, Australia
71 ³⁸GEOMAR Helmholtz Centre for Ocean Research Kiel, Kiel, Germany
72 ³⁹Istituto di Scienze Marine, Consiglio Nazionale delle Ricerche (CNR), Rome, Italy
73 ⁴⁰Université Paris-Saclay, INRAE, AgroParisTech, UMR ECOSYS, Thiverval-Grignon, France
74 ⁴¹Ministry of Education Key Laboratory for Earth System modeling, Department of Earth
75 System Science, Tsinghua University, Beijing, China
76 ⁴²Yale School of Forestry and Environmental Studies, New Haven, CT, USA
77 ⁴³Land Economy, Environment & Society, Scotland's Rural College (SRUC), Edinburgh, UK
78 ⁴⁴Department of Soil, Water, and Climate, University of Minnesota, St Paul, MN, USA
79 ⁴⁵Department of Physical Geography and Ecosystem Science, Lund University, Lund, Sweden
80 ⁴⁶Research Institute for Global Change, JAMSTEC, Yokohama, Japan
81 ⁴⁷Center for Environmental Remote Sensing, Chiba University, Chiba, Japan
82 ⁴⁸Center for Global Change Science, Massachusetts Institute of Technology, Cambridge, MA,
83 USA
84 ⁴⁹Faculty of Science, Vrije Universiteit, Amsterdam, Netherlands.
85 ⁵⁰Scripps Institution of Oceanography, University of California San Diego, La Jolla, USA
86 ⁵¹Department of Forestry, Mississippi State University, Mississippi State, MS, USA

87
88
89
90

91 Nitrous oxide (N₂O), like carbon dioxide, is a long-lived greenhouse gas that accumulates in
92 the atmosphere. The increase in atmospheric N₂O concentrations over the past 150 years
93 has contributed to stratospheric ozone depletion¹ and climate change². Current national
94 inventories do not provide a full picture of N₂O emissions owing to their omission of
95 natural sources and the limitations in methodology for attributing anthropogenic sources.
96 In order to understand the steadily increasing atmospheric burden (about 2 percent per
97 decade) and develop effective mitigation strategies, it is essential to improve quantification
98 and attribution of natural and anthropogenic contributions and their uncertainties. Here
99 we present a global N₂O inventory that incorporates both natural and anthropogenic
100 sources and accounts for the interaction between nitrogen additions and the biochemical
101 processes that control N₂O emissions. We use bottom-up (inventory; statistical
102 extrapolation of flux measurements; process-based land and ocean modelling) and top-
103 down (atmospheric inversion) approaches to provide a comprehensive quantification of
104 global N₂O sources and sinks resulting from 21 natural and human sectors between 1980
105 and 2016. Global N₂O emissions were 17.0 (minimum-maximum: 12.2–23.5) teragrams of
106 nitrogen per year (bottom-up) and 16.9 (15.9–17.7) teragrams of nitrogen per year (top-
107 down) between 2007 and 2016. Global human-induced emissions, which are dominated by
108 nitrogen additions to croplands, increased by 30% over the past four decades to 7.3 (4.2–
109 11.4) teragrams of nitrogen per year. This increase was mainly responsible for the growth
110 in the atmospheric burden. Our findings point to growing N₂O emissions in emerging
111 economies—particularly Brazil, China and India. Analysis of process-based model
112 estimates reveals an emerging N₂O–climate feedback resulting from interactions between
113 nitrogen additions and climate change. The recent growth in N₂O emissions exceeds some

114 **of the highest projected emission scenarios^{3,4}, underscoring the urgency to mitigate N₂O**
115 **emissions.**

116
117 Nitrous oxide (N₂O) is a long-lived stratospheric ozone-depleting substance and greenhouse gas
118 (GHG) with a current atmospheric lifetime of 116±9 years (ref. ¹). The concentration of
119 atmospheric N₂O has increased by over 20% from 270 parts per billion (ppb) in 1750 to 331 ppb
120 in 2018 (Extended Data Fig. 1), with the fastest growth observed in the past five decades^{5,6}. Two
121 key biochemical processes, nitrification and denitrification, control N₂O production in both
122 terrestrial and aquatic ecosystems, and are regulated by multiple environmental and biological
123 factors, such as temperature, water, oxygen, acidity, substrate availability⁷, particularly nitrogen
124 (N) fertilizer use and livestock manure management, and recycling⁸⁻¹⁰. In the coming decades,
125 N₂O emissions are expected to continue increasing due to the growing demand for food, feed,
126 fiber and energy, and a rising source from waste generation and industrial processes^{4,11,12}. Since
127 1990, anthropogenic N₂O emissions have been annually reported by Annex I Parties to the
128 United Nations Framework Convention on Climate Change (UNFCCC). More recently, over 190
129 national signatories to the Paris Agreement are now required to report biannually their national
130 GHG inventory with sufficient detail and transparency to track progress towards their Nationally
131 Determined Contributions. Yet, these inventories do not provide a full picture of N₂O emissions
132 due to their omission of natural sources, the limitations in methodology for attributing
133 anthropogenic sources, and missing data for a number of key regions (e.g., South America,
134 Africa)^{2,9,13}. Moreover, we need a complete account of all human activities that accelerate the
135 global N cycle and that interact with the biochemical processes controlling the fluxes of N₂O in
136 both terrestrial and aquatic ecosystems^{2,8}. Here we present a comprehensive, consistent analysis

137 and synthesis of the global N₂O budget across all sectors, including natural and anthropogenic
138 sources and sinks, using both bottom-up (BU) and top-down (TD) methods and their cross-
139 constraints. Our assessment enhances understanding of the global N cycle and will inform policy
140 development for N₂O mitigation, ideally helping to curb warming to levels consistent with the
141 long-term goal of the Paris Agreement.

142 A reconciling framework (described in Extended Data Fig. 2) was utilized to take full
143 advantage of BU and TD approaches in estimating and constraining sources and sinks of N₂O.
144 BU approaches include emission inventories, spatial extrapolation of field flux measurements,
145 nutrient budget modeling, and process-based modeling for land and ocean fluxes. The TD
146 approaches combine measurements of N₂O mole fractions with atmospheric transport models in
147 statistical optimization frameworks (inversions) to constrain the sources. Here we constructed a
148 total of 43 flux estimates including 30 with BU approaches, five with TD approaches, and eight
149 other estimates with observation and modeling approaches (see Methods; Extended Data Fig. 2).

150 With this extensive data and BU/TD framework, we establish the most comprehensive global
151 and regional N₂O budgets that include 18 sources and different versions of its chemical sink,
152 which are further grouped into six categories (Fig. 1 and Table 1): 1) Natural sources (no
153 anthropogenic effects) including a very small biogenic surface sink, 2) Perturbed fluxes from
154 ecosystems induced by changes in climate, carbon dioxide (CO₂) and land cover, 3) Direct
155 emissions of N additions in the agricultural sector (Agriculture), 4) Other direct anthropogenic
156 sources, which include fossil fuel and industry, waste and waste water, and biomass burning, 5)
157 Indirect emissions from ecosystems that are either downwind or downstream from the initial
158 release of reactive N into the environment, which include N₂O release following transport and
159 deposition of anthropogenic N via the atmosphere or water bodies as defined by the

160 Intergovernmental Panel on Climate Change (IPCC)¹⁴, and 6) The atmospheric chemical sink
161 with one value derived from observations and the other (TD) from the inversion models. To
162 quantify and attribute the regional N₂O budget, we further partition the Earth's ice-free land into
163 ten regions (Fig. 2 and Supplementary Fig. 1). With the construction of these budgets, we
164 explore the relative temporal and spatial importance of multiple sources and sinks driving the
165 atmospheric burden of N₂O, their uncertainties, and interactions between anthropogenic forcing
166 and natural fluxes of N₂O as an emerging climate feedback.

167

168 **The Global N₂O Budget (2007–2016)**

169 The BU and TD approaches give consistent estimates of global total N₂O emissions in the recent
170 decade to well within their respective uncertainties, with values of 17.0 (min-max: 12.2–23.5) Tg
171 N yr⁻¹ and 16.9 (15.9–17.7) Tg N yr⁻¹ for BU and TD sources, respectively. The global calculated
172 atmospheric chemical sink (i.e., N₂O losses via photolysis and reaction with O(¹D) in the
173 troposphere and stratosphere) is 13.5 (12.4–14.6) Tg N yr⁻¹. The imbalance of sources and sinks
174 of N₂O derived from the averaged BU and TD estimates is 4.1 Tg N yr⁻¹. This imbalance agrees
175 well with the observed 2007–2016 increase in atmospheric abundance of 3.8–4.8 Tg N yr⁻¹ (see
176 Methods). Natural sources from soils and oceans contributed 57% of total emissions (mean: 9.7;
177 min-max: 8.0–12.0 Tg N yr⁻¹) for the recent decade according to our BU estimate. We further
178 estimate the natural soil flux at 5.6 (4.9–6.5) Tg N yr⁻¹ and the ocean flux at 3.4 (2.5–4.3) Tg N
179 yr⁻¹ (see Methods).

180 Anthropogenic sources contributed on average 43% to the total N₂O emission (mean: 7.3;
181 min-max: 4.2–11.4 Tg N yr⁻¹), in which direct and indirect emissions from N additions in
182 agriculture and other sectors contributed ~52% and ~18%, respectively. Of the remaining

183 anthropogenic emissions, ~27% were from other direct anthropogenic sources including fossil
184 fuel and industry (~13%), with ~3% from perturbed fluxes caused by climate/CO₂/land cover
185 change.

186

187 **Four Decades of the Global N₂O Budget**

188 The atmospheric N₂O burden increased from 1462 Tg N in the 1980s to 1555 Tg N in the recent
189 decade, with a possible uncertainty ± 20 Tg N. Our results (Table 1) demonstrate that global N₂O
190 emissions have also significantly increased, primarily driven by anthropogenic sources, with
191 natural sources relatively steady throughout the study period. Our BU and TD global N₂O
192 emissions are comparable in magnitude during 1998–2016, but TD results imply a larger inter-
193 annual variability (1.0 Tg N yr⁻¹; Extended Data Fig. 3a). BU and TD approaches diverge in the
194 magnitude of land versus ocean emissions, although they are consistent with respect to trends.
195 Specifically, the BU land estimate during 1998–2016 was on average 1.8 Tg N yr⁻¹ higher than
196 the TD estimate, but showed a slightly slower increasing rate of 0.8 ± 0.2 Tg N yr⁻¹ per decade
197 (95% confidence interval; $P < 0.05$) compared to 1.1 ± 0.6 Tg N yr⁻¹ per decade ($P < 0.05$) from
198 TD (Extended Data Fig. 3b). Since 2005, the difference in the magnitude of emissions between
199 the two approaches has become smaller due to a large TD-inferred emission increase,
200 particularly in South America, Africa, and East Asia (Extended Data Fig. 3d, f, i). Oceanic N₂O
201 emissions from BU [3.6 (2.7–4.5) Tg N yr⁻¹] indicate a slight decline at a rate of 0.06 Tg N yr⁻¹
202 per decade ($P < 0.05$), while the TD approach gave a higher but stable value of 5.1 (3.4–7.1) Tg
203 N yr⁻¹ during 1998–2016 (Table 1).

204 Based on BU approaches, anthropogenic N₂O emissions increased from 5.6 (3.6–8.7) Tg N yr⁻¹
205 ¹ in the 1980s to 7.3 (4.2–11.4) Tg N yr⁻¹ in the recent decade at a rate of 0.6 ± 0.2 Tg N yr⁻¹ per

206 decade ($P < 0.05$). Up to 87% of this increase is from direct emission from agriculture (71%) and
207 indirect emission from anthropogenic N additions into soils (16%). Direct soil emission from
208 fertilizer applications is the major source for agricultural emission increases, followed by a small
209 but significant increase in emissions from livestock manure and aquaculture. The model-based
210 estimates of direct soil emissions¹⁵⁻¹⁷ exhibit a faster increase than the three inventories used in
211 our study (see Methods; Extended Data Fig. 4a), which is largely attributed to the interactive
212 effects between climate change and N additions as well as spatio-temporal variability in
213 environmental factors such as rainfall and temperature that modulate the N₂O yield from
214 nitrification and denitrification. This result is in line with the elevated emission factor (EF)
215 deduced from the TD estimates, in which the inversion-based soil emissions increased at a faster
216 rate than suggested by the IPCC Tier 1 EF¹⁴ (which assumes a linear response), especially after
217 2009 (ref. ¹⁸). The remaining causes of the increase are attributed to other direct anthropogenic
218 sources (6%) and perturbed fluxes from climate/CO₂/land cover change (8%). The part of fossil
219 fuel and industry emissions decreased rapidly over 1980–2000 largely due to the installation of
220 emissions abatement equipment in industrial facilities producing nitric and adipic acid. However,
221 after 2000 such emissions began to increase slowly due to rising fossil fuel combustion
222 (Extended Data Fig. 5a-b).

223 Our analysis of process-based model estimates indicates that soil N₂O emissions accelerated
224 substantially due to climate change since the early 1980s, which has offset the reduction due to
225 elevated CO₂ concentration (Extended Data Fig. 6a). Elevated CO₂ enhances plant growth and
226 thus increases N uptake, which in turn decreases soil N₂O emissions^{16,19}. Land conversion from
227 tropical mature forests with higher N₂O emissions to pastures and other unfertilized agricultural
228 lands has significantly reduced global natural N₂O emissions^{11,20,21}. This decrease, however, was

229 partly offset by an increase in soil N₂O emissions attributable to the temporary rise of emissions
230 following deforestation (post-deforestation pulse effect) and background emissions from
231 converted croplands or pastures²¹ (see Methods; Extended Data Fig. 7).

232 From the ensemble of process-based land model emissions^{15,16}, we estimate a global
233 agricultural soil EF of 1.8% (1.3%–2.3%), which is significantly larger than the IPCC Tier-1
234 default for direct emission of 1%. This higher EF, derived from process-based models, suggests a
235 strong interactive effect between N additions and other global environmental changes (Table 1,
236 Perturbed fluxes from climate, atmospheric CO₂, and land cover change). Previous field
237 experiments reported a better fit to local observations of soil N₂O emissions when assuming a
238 non-linear response to fertilizer N inputs under varied climate and soil conditions^{17,22}. The non-
239 linear response is likely also associated with long-term N accumulation in agricultural soils from
240 N fertilizer use and in aquatic systems from N loads (the legacy effect)^{18,23}, which provides more
241 substrate for microbial processes^{18,24}. The increasing N₂O emissions estimated by process-based
242 models¹⁶ also suggest that recent climate change (particularly warming) may have boosted soil
243 nitrification and denitrification processes, contributing to the growing trend in N₂O emissions
244 together with rising N additions to agricultural soils^{16,25-27} (Extended Data Fig. 8).

245

246 **Regional N₂O Budgets (2007–2016)**

247 BU approaches give estimates of N₂O emissions in the five source categories, while TD
248 approaches only provide total emissions (Fig. 2). BU and TD approaches indicate that Africa was
249 the largest N₂O source in the last decade, followed by South America (Fig. 2). BU and TD
250 approaches agree well in the magnitudes and trends of N₂O emissions from South Asia and
251 Oceania (Extended Data Fig. 3j, l). For the remaining regions, BU and TD estimates are

252 comparable in their trends but diverge in their source strengths. Clearly, much more work on
253 regional N₂O budgets is needed, particularly for South America and Africa where we see larger
254 differences between BU and TD estimates and larger uncertainty in each approach. Advancing
255 the understanding and model representation of key processes responsible for N₂O emissions from
256 land and ocean are priorities for reducing uncertainties in BU estimates. Atmospheric
257 observations in underrepresented regions of the world and better atmospheric transport models
258 are essential for uncertainty reduction in TD estimates, while more accurate activity data and
259 robust EFs are critical for GHG inventories (See Methods for additional discussion on
260 uncertainty).

261 Based on the Global N₂O Model Intercomparison Project (NMIP) estimates¹⁶, natural soil
262 emissions (to different extents) dominated in tropical and sub-tropical regions. Soil N₂O
263 emissions in the tropics ($0.1 \pm 0.04 \text{ g N m}^{-2} \text{ yr}^{-1}$) are about 50% higher than the global average,
264 since many lowland, highly-weathered tropical soils have excess N relative to phosphorus²⁰.
265 Total anthropogenic emissions in the ten terrestrial regions were highest in East Asia (1.5;
266 0.8–2.6 Tg N yr⁻¹), followed by North America, Africa, and Europe. High direct agricultural N₂O
267 emissions can be attributed to large-scale synthetic N fertilizer applications in East Asia, Europe,
268 South Asia, and North America, which together consume over 80% of the world's synthetic N
269 fertilizers²⁸. In contrast, direct agricultural emissions from Africa and South America are mainly
270 induced by livestock manure that is deposited in pastures and rangelands^{28,29}. East Asia
271 contributed 71%–79% of global aquaculture N₂O emissions; South Asia and Southeast Asia
272 together contributed 10%–20% (refs. ^{30,31}). Indirect emissions play a moderate role in the total
273 N₂O budget, with the highest emission in East Asia (0.3; 0.1–0.5 Tg N yr⁻¹). Other direct

274 anthropogenic sources together contribute N₂O emissions of approximately 0.2–0.4 Tg N yr⁻¹ in
275 East Asia, Africa, North America, and Europe.

276 Both BU and TD estimates of ocean N₂O emissions for northern, tropical, and southern ocean
277 regions (90°–30°N, 30°N–30°S, and 30°–90°S, respectively) reveal that the tropical oceans
278 contribute over 50% to the global oceanic source. In particular, the upwelling regions of the
279 equatorial Pacific, Indian and tropical Atlantic (Fig. 3) provide significant sources of N₂O³²⁻³⁴.
280 BU estimates suggest the southern ocean is the second largest regional contributor with
281 emissions about twice as high as from the northern oceans (53% tropical oceans, 31% southern
282 oceans, 17% northern oceans), in line with their area, while the TD estimates suggest
283 approximately equal contributions from the southern and northern oceans.

284

285 **Four Decades of Anthropogenic N₂O Emissions**

286 Trends in anthropogenic emissions varied among regions (Fig. 3). Fluxes from Europe and
287 Russia decreased by a total of 0.6 (0.5–0.7) Tg N yr⁻¹ over the past 37 years (1980–2016). The
288 decrease in Europe is associated with successful emissions abatement in industry as well as
289 agricultural policies, while the decrease in Russia is associated with the collapse of the
290 agricultural cooperative system after 1990. In contrast, fluxes from the remaining eight regions
291 increased by a total of 2.9 (2.4–3.4) Tg N yr⁻¹ (Fig. 3), of which 34% came from East Asia, 18%
292 from Africa, 18% from South Asia, 13% from South America, only 6% from North America,
293 and with remaining increases due to other regions.

294 The relative importance of each anthropogenic source to the total emission increase differs
295 among regions. East Asia, South Asia, Africa, and South America show larger increases in total
296 agricultural N₂O emissions (direct and indirect) compared to the remaining six regions during

297 1980–2016 (Fig. 3). Southeast Asia, North America, and Middle East also show increasing direct
298 N₂O emissions but to smaller extent. Rising indirect emissions in these four regions (East Asia,
299 South Asia, Africa, and South America) on average constitute 20% of total agricultural N₂O
300 emissions and are largely induced by the considerable increase in fertilizer N inputs to
301 agricultural soils^{35,36}. The most rapid increase in emissions from other direct anthropogenic
302 sources was found in East Asia, primarily owing to the fast-growing industrial emissions. Africa
303 and South Asia show a fast emission increase due to emissions from fossil fuel and industry and
304 waste and waste water.

305 Our findings point to growing N₂O emissions in emerging economies, particularly Brazil,
306 China, and India. For example, we find here that the substantial increases in livestock manure
307 left on pasture and in fertilizer use caused a ~120% increase in Brazilian agricultural N₂O
308 emissions during 1980–2016 (Extended Data Fig. 9). In addition to fertilizer applications, global
309 livestock manure production has been growing steadily, in line with increased livestock
310 numbers^{15,28}. Rising demand for meat and dairy products has significantly increased global N₂O
311 emissions from livestock manure production and management associated with the expansion of
312 pastures and grazing land³⁷. Meanwhile, expansion of feed crop production to support the growth
313 of livestock could further enhance global N₂O emissions^{37,38}. Likewise, increasing demand for
314 fish has triggered a five-fold increase in global aquaculture production since the late 1980s³⁹,
315 with demand projected to increase further⁴⁰, although this remains a small fraction (<1%) of total
316 N₂O emissions.

317 The acceleration of global N₂O emissions resulting from anthropogenic sources is apparent in
318 both BU and TD results and currently tracks the highest Representative Concentration Pathway
319 (RCP8.5)⁴ in the fifth assessment report (AR5) of IPCC² and exceeds all the Shared

320 Socioeconomic Pathways (SSPs)³ in CMIP6 for the sixth assessment report (AR6) of IPCC (Fig.
321 4). Observed atmospheric N₂O concentrations are beginning to exceed predicted levels across all
322 scenarios. Emissions need to be reduced to a level that is consistent with or below that in RCP2.6
323 or SSP1-2.6 in order to limit warming well below the 2° C target of the Paris Agreement. Failure
324 to include N₂O within climate mitigation strategies will necessitate even greater abatement of
325 CO₂ and CH₄. Although N₂O mitigation is difficult because N is the key-limiting nutrient in the
326 agricultural production, this study demonstrates that effective mitigation actions have reduced
327 emissions in some regions, such as Europe, through technological improvements in industry and
328 improved N use efficiency in agriculture.

329 There are a number of mitigation options in the agriculture sector available for immediate
330 deployment, including increased N use efficiency in (i) animal production through tuning of feed
331 rations to reduce N excretion, and (ii) in crop production through precision delivery of N
332 fertilizers, split applications and better timing to match N applications to crop demand,
333 conservation tillage, prevention of waterlogging, and the use of nitrification inhibitors^{43,44}.
334 Success stories include the stabilization or reduction of N₂O emissions through improving N use
335 efficiency in the United States and Europe, while maintaining or even increasing crop yields^{44,45}.
336 There is every reason to expect that additional implementation of more sustainable practices and
337 emerging technologies will lead to further reductions in these regions. For example, N₂O
338 emissions from European agricultural soils decreased by 21% between 1990 and 2010, a decline
339 attributable to the implementation of the Nitrates Directive (an agricultural policy favoring
340 optimization and reduction of fertilizer use as well as water protection legislation)⁴⁶. For regions
341 where emissions are growing, an immediate opportunity lies in the reduction of excess fertilizer
342 use along with the implementation of more sustainable agricultural practices that together have

343 been shown to increase crop yields, reduce N₂O emissions, increase water quality, and increase
344 farm income⁴⁷. In addition, N₂O emissions can be efficiently abated in the chemical
345 industry^{11,43,48,49}, as has been achieved successfully in nitric acid plants in the European Union
346 where industrial N₂O emissions dropped from 11% to 3% of total emissions between 2007 and
347 2012 (ref. ⁴⁶). Additional available strategies to reduce N₂O emissions include promoting lower
348 meat consumption in some parts of the world⁹ and reducing food waste¹¹.

349 We present the most comprehensive global N₂O budget to date, with a detailed sectorial and
350 regional attribution of sources and sinks. Each of the past four decades had higher global N₂O
351 emissions than the previous one, and in all, agricultural activities dominated the growth in
352 emissions. Total industrial emissions have been quite stable with increased emissions from the
353 fossil fuel sector offset to some extent by the decline in emissions in other industrial sectors as a
354 result of successful abatement policies. We also highlight a number of complex interactions
355 between N₂O fluxes and human-driven changes whose impact on the global atmospheric N₂O
356 growth rate was previously unknown. Those interactions include the effects of climate change,
357 increasing atmospheric CO₂, and deforestation. Cumulatively, these exert a relatively small
358 effect on the overall N₂O growth, however, individual flux components, such as the growing
359 positive climate-N₂O feedback, are significant. These fluxes are not currently included in the
360 national GHG reporting. We further find that Brazil, China, and India dominate the regional
361 contributions to the increase in global N₂O emissions over the most recent decade. Our extensive
362 database and modelling capability fill current gaps in national and regional emissions
363 inventories. Future research is needed to further constrain complex biogeochemical interactions
364 between natural/anthropogenic fluxes and global environmental changes, which could lead to
365 significant feedbacks in the future. Reducing excess N applications to croplands and adopting

366 precision fertilizer application methods provide the largest immediate opportunities for N₂O
367 emissions abatement.

368

369 **References**

- 370 1 Prather, M. J. *et al.* Measuring and modeling the lifetime of nitrous oxide including its
371 variability. *Journal of Geophysical Research: Atmospheres* **120**, 5693-5705 (2015).
- 372 2 Ciais, P. *et al.* in *Climate Change 2013: The Physical Science Basis. Contribution of*
373 *Working Group I to the Fifth Assessment Report of the Intergovernmental Panel on*
374 *Climate Change* 465-570 (Cambridge University Press, 2014).
- 375 3 Gidden, M. J. *et al.* Global emissions pathways under different socioeconomic scenarios
376 for use in CMIP6: a dataset of harmonized emissions trajectories through the end of the
377 century. *Geoscientific Model Development* **12**, 1443-1475 (2019).
- 378 4 Davidson, E. A. Representative concentration pathways and mitigation scenarios for
379 nitrous oxide. *Environmental Research Letters* **7**, 024005 (2012).
- 380 5 Hall, B., Dutton, G. & Elkins, J. The NOAA nitrous oxide standard scale for atmospheric
381 observations. *Journal of Geophysical Research: Atmospheres* **112**, D09305 (2007).
- 382 6 Prinn, R. G. *et al.* History of chemically and radiatively important atmospheric gases
383 from the Advanced Global Atmospheric Gases Experiment (AGAGE). *Earth System*
384 *Science Data* **10**, 985-1018 (2018).
- 385 7 Butterbach-Bahl, K., Baggs, E. M., Dannenmann, M., Kiese, R. & Zechmeister-
386 Boltenstern, S. Nitrous oxide emissions from soils: how well do we understand the
387 processes and their controls? *Phil. Trans. R. Soc. B* **368**, 20130122 (2013).
- 388 8 Tian, H. *et al.* The terrestrial biosphere as a net source of greenhouse gases to the
389 atmosphere. *Nature* **531**, 225-228 (2016).
- 390 9 UNEP. Drawing down N₂O to protect climate and the ozone layer. Report No.
391 9280733583, (United Nations Environment Programme (UNEP), 2013).
- 392 10 Park, S. *et al.* Trends and seasonal cycles in the isotopic composition of nitrous oxide
393 since 1940. *Nature Geoscience* **5**, 261-265 (2012).
- 394 11 Davidson, E. A. & Kanter, D. Inventories and scenarios of nitrous oxide emissions.
395 *Environmental Research Letters* **9**, 105012 (2014).
- 396 12 Reay, D. S. *et al.* Global agriculture and nitrous oxide emissions. *Nature Climate Change*
397 **2**, 410-416 (2012).
- 398 13 Syakila, A. & Kroeze, C. The global nitrous oxide budget revisited. *Greenhouse Gas*
399 *Measurement and Management* **1**, 17-26 (2011).
- 400 14 IPCC. 2006 IPCC Guidelines for National Greenhouse Gas Inventories., (Japan on behalf
401 of the IPCC, Hayama, Japan, 2006).
- 402 15 Dangal, S. R. *et al.* Global nitrous oxide emissions from pasturelands and rangelands:
403 Magnitude, spatio-temporal patterns and attribution. *Global Biogeochemical Cycles* **33**,
404 200-222 (2019).
- 405 16 Tian, H. Q. *et al.* Global soil nitrous oxide emissions since the preindustrial era estimated
406 by an ensemble of terrestrial biosphere models: Magnitude, attribution, and uncertainty.
407 *Global Change Biology* **25**, 640-659 (2019).

- 408 17 Wang, Q. *et al.* Data-driven estimates of global nitrous oxide emissions from croplands.
409 *National Science Review* **7**, 441-452 (2020).
- 410 18 Thompson, R. L. *et al.* Acceleration of global N₂O emissions seen from two decades of
411 atmospheric inversion. *Natural Climate Change* **9**, 993-998 (2019).
- 412 19 Zaehle, S., Ciais, P., Friend, A. D. & Prieur, V. Carbon benefits of anthropogenic reactive
413 nitrogen offset by nitrous oxide emissions. *Nature Geoscience* **4**, 601-605 (2011).
- 414 20 Davidson, E. A. *et al.* Recuperation of nitrogen cycling in Amazonian forests following
415 agricultural abandonment. *Nature* **447**, 995-998 (2007).
- 416 21 Verchot, L. V. *et al.* Land use change and biogeochemical controls of nitrogen oxide
417 emissions from soils in eastern Amazonia. *Global Biogeochemical Cycles* **13**, 31-46
418 (1999).
- 419 22 Shcherbak, I., Millar, N. & Robertson, G. P. Global metaanalysis of the nonlinear
420 response of soil nitrous oxide (N₂O) emissions to fertilizer nitrogen. *Proceedings of the*
421 *National Academy of Sciences* **111**, 9199-9204 (2014).
- 422 23 Van Meter, K. J., Basu, N. B., Veenstra, J. J. & Burras, C. L. The nitrogen legacy:
423 emerging evidence of nitrogen accumulation in anthropogenic landscapes. *Environmental*
424 *Research Letters* **11**, 035014 (2016).
- 425 24 Firestone, M. K. & Davidson, E. A. Microbiological basis of NO and N₂O production and
426 consumption in soil. *Exchange of trace gases between terrestrial ecosystems the*
427 *atmosphere* **47**, 7-21 (1989).
- 428 25 Griffis, T. J. *et al.* Nitrous oxide emissions are enhanced in a warmer and wetter world.
429 *Proceedings of the National Academy of Sciences* **114**, 12081-12085 (2017).
- 430 26 Pärn, J. *et al.* Nitrogen-rich organic soils under warm well-drained conditions are global
431 nitrous oxide emission hotspots. *Nature Communications* **9**, 1135 (2018).
- 432 27 Smith, K. The potential for feedback effects induced by global warming on emissions of
433 nitrous oxide by soils. *Global Change Biology* **3**, 327-338 (1997).
- 434 28 FAOSTAT. The Food and Agriculture Organization of the United Nations Statistics:
435 Emissions-Agriculture, Emissions Land Use Trade (Crops and livestock products),
436 Population, Agri-Environmental Indicators (Livestock Manure) (2019).
- 437 29 Xu, R. *et al.* Increased nitrogen enrichment and shifted patterns in the world's grassland:
438 1860–2016. *Earth System Science Data* **11**, 175-187 (2019).
- 439 30 Beusen, A. H., Bouwman, A. F., Van Beek, L. P., Mogollón, J. M. & Middelburg, J. J.
440 Global riverine N and P transport to ocean increased during the 20th century despite
441 increased retention along the aquatic continuum. *Biogeosciences* **13**, 2441-2451 (2016).
- 442 31 MacLeod, M., Hasan, M. R., Robb, D. H. F. & Mamun-Ur-Rashid, M. Quantifying and
443 mitigating greenhouse gas emissions from global aquaculture. *FAO, Rome* (2019).
- 444 32 Buitenhuis, E. T., Suntharalingam, P. & Le Quéré, C. Constraints on global oceanic
445 emissions of N₂O from observations and models. *Biogeosciences* **15**, 2161-2175 (2018).
- 446 33 Manizza, M., Keeling, R. F. & Nevison, C. D. On the processes controlling the seasonal
447 cycles of the air–sea fluxes of O₂ and N₂O: A modelling study. *Tellus B: Chemical and*
448 *Physical Meteorology* **64**, 18429 (2012).
- 449 34 Martinez-Rey, J., Bopp, L., Gehlen, M., Tagliabue, A. & Gruber, N. Projections of
450 oceanic N₂O emissions in the 21st century using the IPSL Earth system model.
451 *Biogeosciences* **12**, 4133-4148 (2015).
- 452 35 Maavara, T. *et al.* Nitrous oxide emissions from inland waters: Are IPCC estimates too
453 high? *Global Change Biology* **25**, 473-488 (2019).

454 36 Yao, Y. *et al.* Increased global nitrous oxide emissions from streams and rivers in the
455 Anthropocene. *Natural Climate Change* **10**, 138-142 (2020).

456 37 Gerber, P. J. *et al.* *Tackling climate change through livestock: a global assessment of*
457 *emissions and mitigation opportunities.* *FAO* (2013).

458 38 Herrero, M. *et al.* Biomass use, production, feed efficiencies, and greenhouse gas
459 emissions from global livestock systems. *Proceedings of the National Academy of*
460 *Sciences* **110**, 20888-20893 (2013).

461 39 Yuan, J. *et al.* Rapid growth in greenhouse gas emissions from the adoption of industrial-
462 scale aquaculture. *Nature Climate Change* **9**, 318-322 (2019).

463 40 Froehlich, H. E., Runge, C. A., Gentry, R. R., Gaines, S. D. & Halpern, B. S.
464 Comparative terrestrial feed and land use of an aquaculture-dominant world. *Proceedings*
465 *of the National Academy of Sciences* **115**, 5295-5300 (2018).

466 41 O'Neill, B. C. *et al.* The Scenario Model Intercomparison Project (ScenarioMIP) for
467 CMIP6. *Geoscience Model Development* **9**, 3461-3482 (2016).

468 42 Gütschow, J. *et al.* The PRIMAP-hist national historical emissions time series. *Earth*
469 *System Science Data* **8**, 571-603 (2016).

470 43 Winiwarter, W., Höglund-Isaksson, L., Klimont, Z., Schöpp, W. & Amann, M. Technical
471 opportunities to reduce global anthropogenic emissions of nitrous oxide. *Environmental*
472 *Research Letters* **13**, 014011 (2018).

473 44 Zhang, X. *et al.* Managing nitrogen for sustainable development. *Nature* **528**, 51-59
474 (2015).

475 45 Mueller, N. D. *et al.* Declining spatial efficiency of global cropland nitrogen allocation.
476 *Global Biogeochemical Cycles* **31**, 245-257 (2017).

477 46 European Environment Agency. Annual European Union greenhouse gas inventory 1990-
478 2017 and inventory report 2019. *Submission under the United Nations Framework*
479 *Convention on Climate Change and the Kyoto Protocol, Copenhagen, DK* (2019).

480 47 Cui, Z. *et al.* Pursuing sustainable productivity with millions of smallholder farmers.
481 *Nature* **555**, 363-366 (2018).

482 48 Kanter, D. *et al.* A post-Kyoto partner: considering the stratospheric ozone regime as a
483 tool to manage nitrous oxide. *Proceedings of the National Academy of Sciences* **110**,
484 4451-4457 (2013).

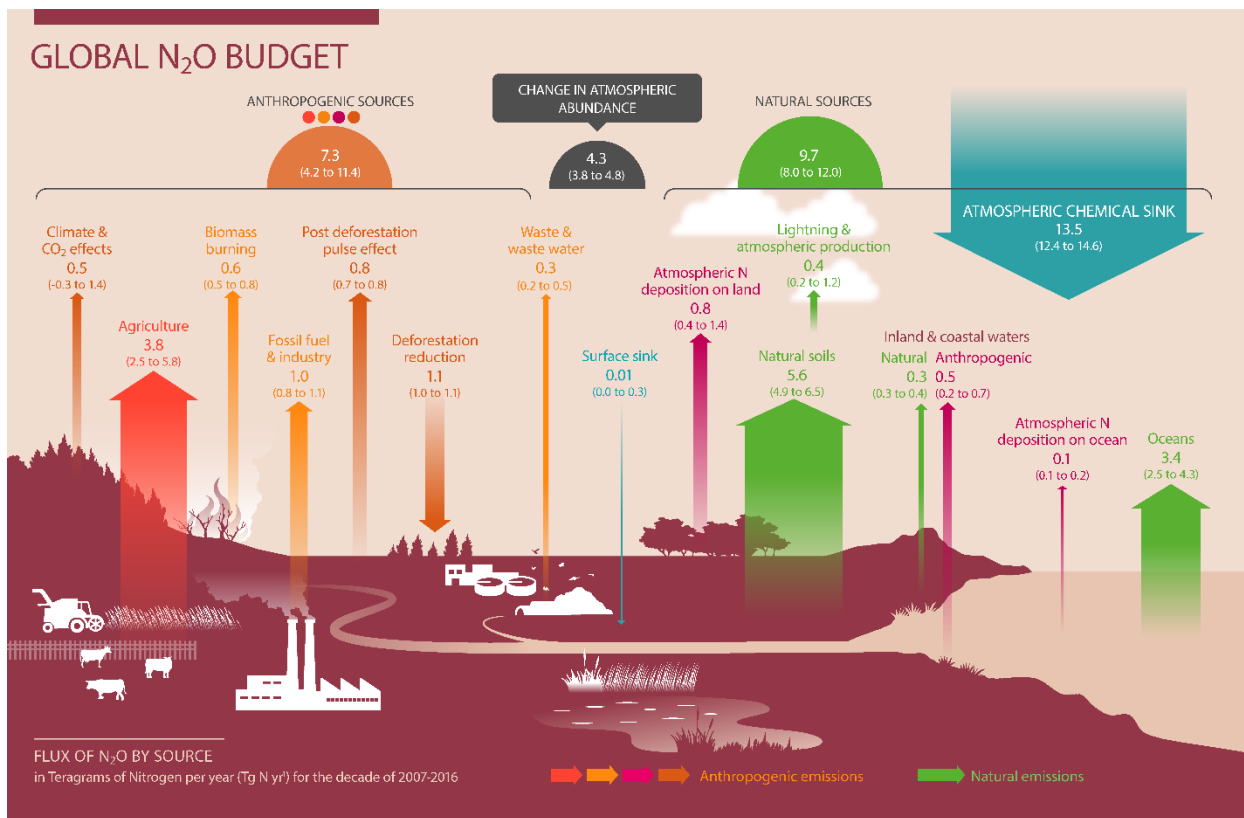
485 49 Schneider, L., Lazarus, M. & Kollmuss, A. J. S. M. S. E. I. Industrial N₂O projects under
486 the CDM: Adipic acid-A case of carbon leakage. *Stockholm Environment Institute*
487 (2010).

488
489
490
491
492
493
494
495

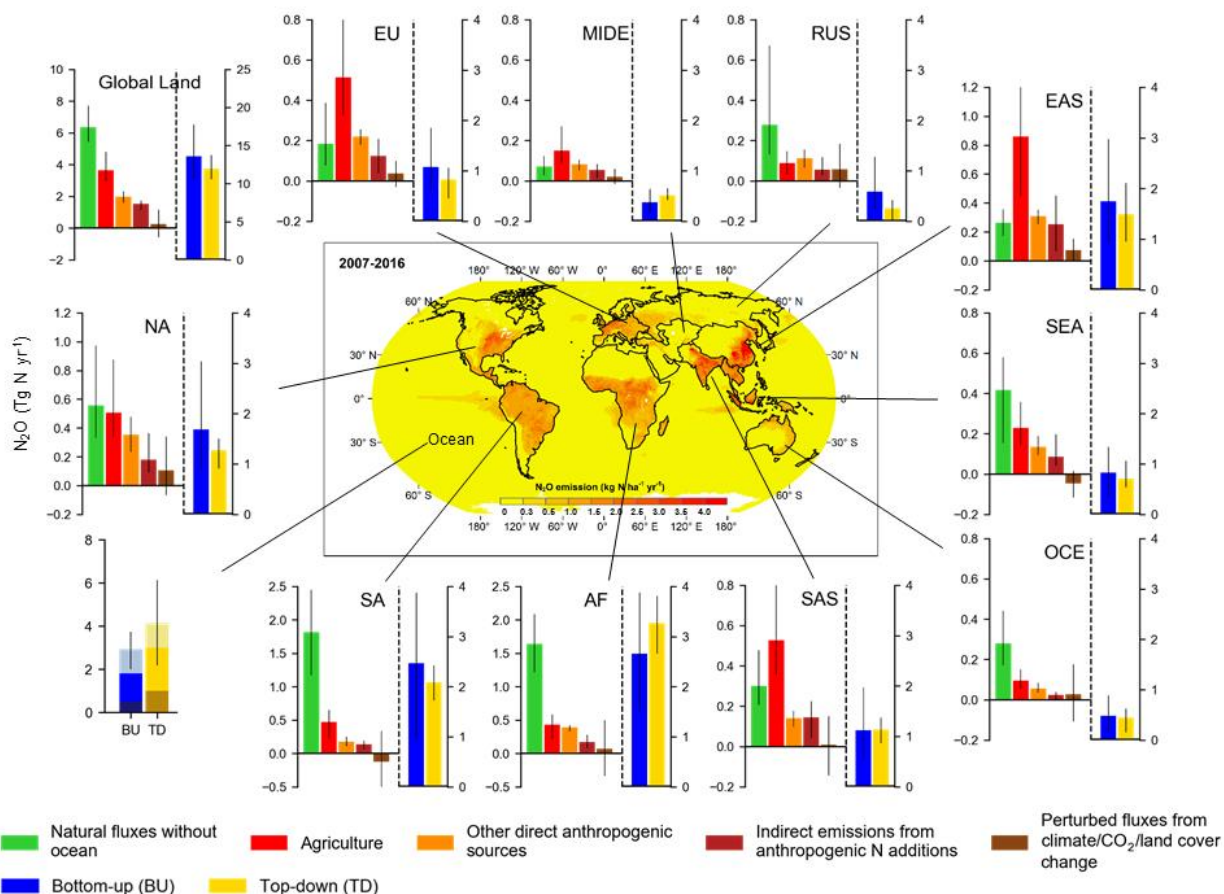
496 **Table 1** The global N₂O budget in the 1980s, 1990s, 2000s, and 2007–2016.

		the 1980s			the 1990s			the 2000s			2007-2016		
<i>Anthropogenic sources</i>		mean	min	max	mean	min	max	mean	min	max	mean	min	max
Direct emissions of N additions in the agricultural sector (Agriculture)	Direct soil emissions	1.5	0.9	2.6	1.7	1.1	3.1	2.0	1.3	3.4	2.3	1.4	3.8
	Manure left on pasture	0.9	0.7	1.0	1.0	0.7	1.1	1.1	0.8	1.2	1.2	0.9	1.3
	Manure management	0.3	0.2	0.4	0.3	0.2	0.4	0.3	0.2	0.5	0.3	0.2	0.5
	Aquaculture	0.01	0.00	0.03	0.03	0.01	0.1	0.1	0.02	0.2	0.1	0.02	0.2
	sub-total	2.6	1.8	4.1	3.0	2.1	4.8	3.4	2.3	5.2	3.8	2.5	5.8
Other direct anthropogenic sources	Fossil fuel and industry	0.9	0.8	1.1	0.9	0.9	1.0	0.9	0.8	1.0	1.0	0.8	1.1
	Waste and waste water	0.2	0.1	0.3	0.3	0.2	0.4	0.3	0.2	0.4	0.3	0.2	0.5
	Biomass burning	0.7	0.7	0.7	0.7	0.6	0.8	0.6	0.6	0.6	0.6	0.5	0.8
	sub-total	1.8	1.6	2.1	1.9	1.7	2.1	1.8	1.6	2.1	1.9	1.6	2.3
Indirect emissions from anthropogenic N additions	Inland waters, estuaries, coastal zones	0.4	0.2	0.5	0.4	0.2	0.5	0.4	0.2	0.6	0.5	0.2	0.7
	Atmospheric N deposition on land	0.6	0.3	1.2	0.7	0.4	1.4	0.7	0.4	1.3	0.8	0.4	1.4
	Atmospheric N deposition on ocean	0.1	0.1	0.2	0.1	0.1	0.2	0.1	0.1	0.2	0.1	0.1	0.2
	sub-total	1.1	0.6	1.9	1.2	0.7	2.1	1.2	0.6	2.1	1.3	0.7	2.2
Perturbed fluxes from climate/CO ₂ /land cover change	CO ₂ effect	-0.2	-0.3	0.0	-0.2	-0.4	0.0	-0.3	-0.5	0.1	-0.3	-0.6	0.1
	Climate effect	0.4	0.0	0.8	0.5	0.1	0.9	0.7	0.3	1.2	0.8	0.3	1.3
	Post-deforestation pulse effect	0.7	0.6	0.8	0.7	0.6	0.8	0.7	0.7	0.8	0.8	0.7	0.8
	Long-term effect of reduced mature forest area	-0.8	-0.8	-0.9	-0.9	-0.8	-1.0	-1.0	-0.9	-1.1	-1.1	-1.0	-1.1
	sub-total	0.1	-0.4	0.7	0.1	-0.5	0.7	0.2	-0.4	0.9	0.2	-0.6	1.1
Anthropogenic total		5.6	3.6	8.7	6.2	3.9	9.7	6.7	4.1	10.3	7.3	4.2	11.4
Natural fluxes													
Natural soils baseline		5.6	4.9	6.6	5.6	4.9	6.5	5.6	5.0	6.5	5.6	4.9	6.5
Ocean baseline		3.6	3.0	4.4	3.5	2.8	4.4	3.5	2.7	4.3	3.4	2.5	4.3
Natural (Inland waters, estuaries, coastal zones)		0.3	0.3	0.4	0.3	0.3	0.4	0.3	0.3	0.4	0.3	0.3	0.4
Lightning and atmospheric production		0.4	0.2	1.2	0.4	0.2	1.2	0.4	0.2	1.2	0.4	0.2	1.2
Surface sink		-0.01	0.00	-0.3	-0.01	0.00	-0.3	-0.01	0.00	-0.3	-0.01	0.00	-0.3
Natural total		9.9	8.5	12.2	9.8	8.3	12.1	9.8	8.2	12.0	9.7	8.0	12.0
Bottom-up total source		15.5	12.1	20.9	15.9	12.2	21.7	16.4	12.3	22.4	17.0	12.2	23.5
<i>Top-down Ocean</i>								5.1	3.1	7.2	5.1	3.4	7.1
<i>Top-down Land</i>								10.8	9.3	12.5	11.8	10.6	13.8
Top-down total source								15.9	15.1	16.9	16.9	15.9	17.7
<i>Top-down Statospheric sink</i>								12.1	11.4	13.1	12.4	11.7	13.3
Observed atmospheric chemical sink*								13.3	12.2	14.4	13.5	12.4	14.6
Change in atmospheric abundance**								3.7	3.2	4.2	4.3	3.8	4.8
Atmospheric burden		1462	1442	1482	1493	1472	1514	1531	1510	1552	1555	1533	1577

497 Note: BU estimates include four categories of anthropogenic sources (red for agriculture, orange for
498 other direct anthropogenic sources, maroon for indirect emissions from anthropogenic N additions, and
499 brown for perturbed fluxes from climate/CO₂/land cover change) and one category for natural sources
500 and sinks (green). The sources and sinks of N₂O are given in Tg N yr⁻¹. The atmospheric burden is given
501 in Tg N. *calculated from satellite observations with a photolysis model (about 1% of this sink
502 occurs in the troposphere). **Calculated from the combined NOAA and AGAGE record of surface N₂O,
503 and adopting the uncertainty of the IPCC AR5 (Chapter 6)². Detailed information on calculating each
504 sub-category is shown in Supplementary Tables 1–13.

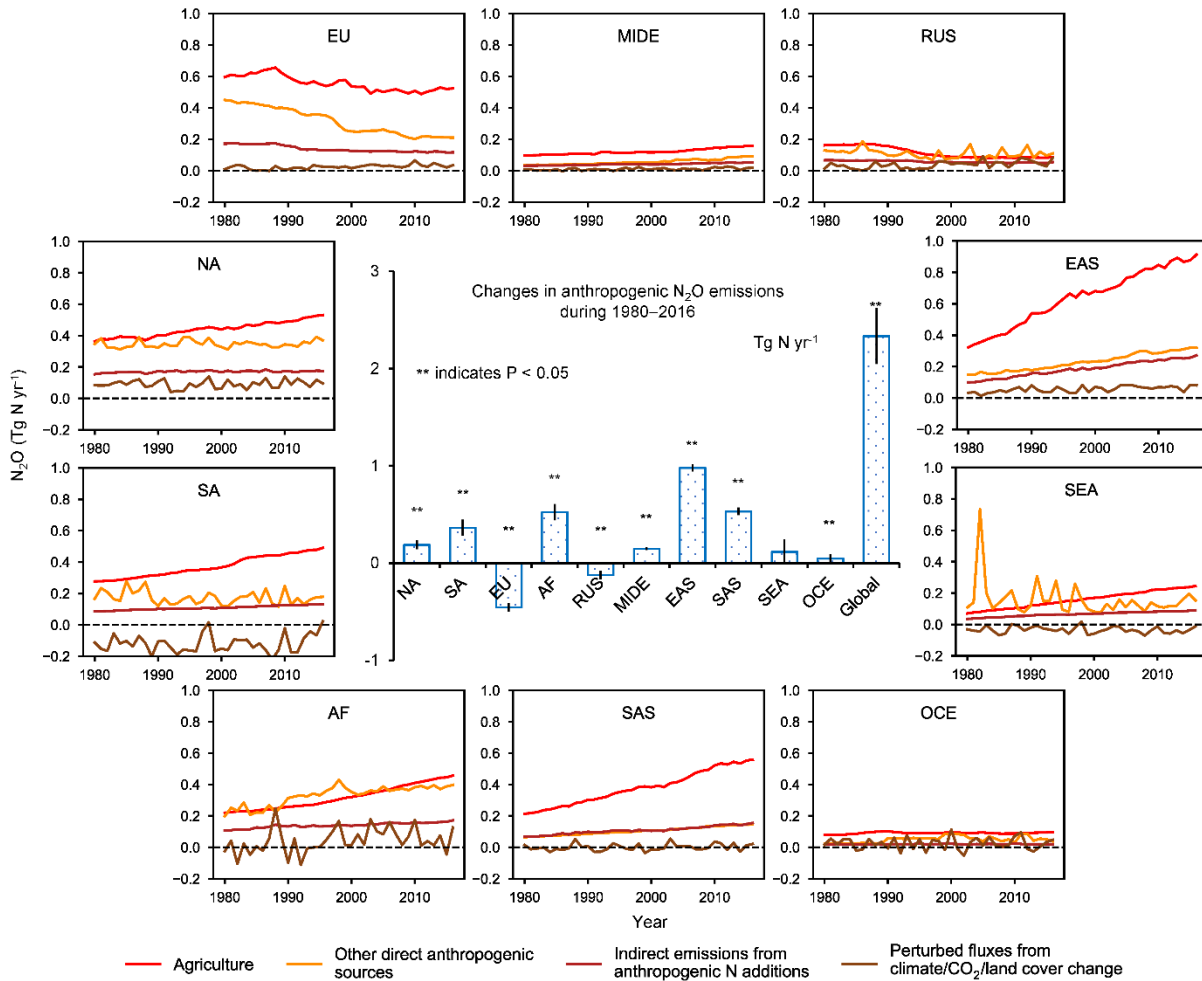


505
 506 **Fig. 1 Global N₂O budget for the recent decade (2007–2016).** The red arrow represents direct
 507 emissions of N additions in the agricultural sector (Agriculture). The orange arrows represent emissions
 508 from other direct anthropogenic sources. The maroon arrows represent indirect emissions from
 509 anthropogenic N additions. The brown arrows represent perturbed fluxes from climate/CO₂/land cover
 510 change effects. The green arrows represent natural source. The anthropogenic and natural N₂O sources
 511 are derived from BU estimates. The blue arrows represent surface sink and observed atmospheric
 512 chemical sink of which about 1% occurs in the troposphere. The total budget (sources + sinks) does not
 513 exactly match the observed atmospheric accumulation, because each of the terms has been derived
 514 independently and we do not force top-down agreement by rescaling the terms. This imbalance readily
 515 falls within the overall uncertainty in closing the N₂O budget, as reflected in each of the terms. The N₂O
 516 sources and sinks are given in Tg N yr⁻¹.
 517



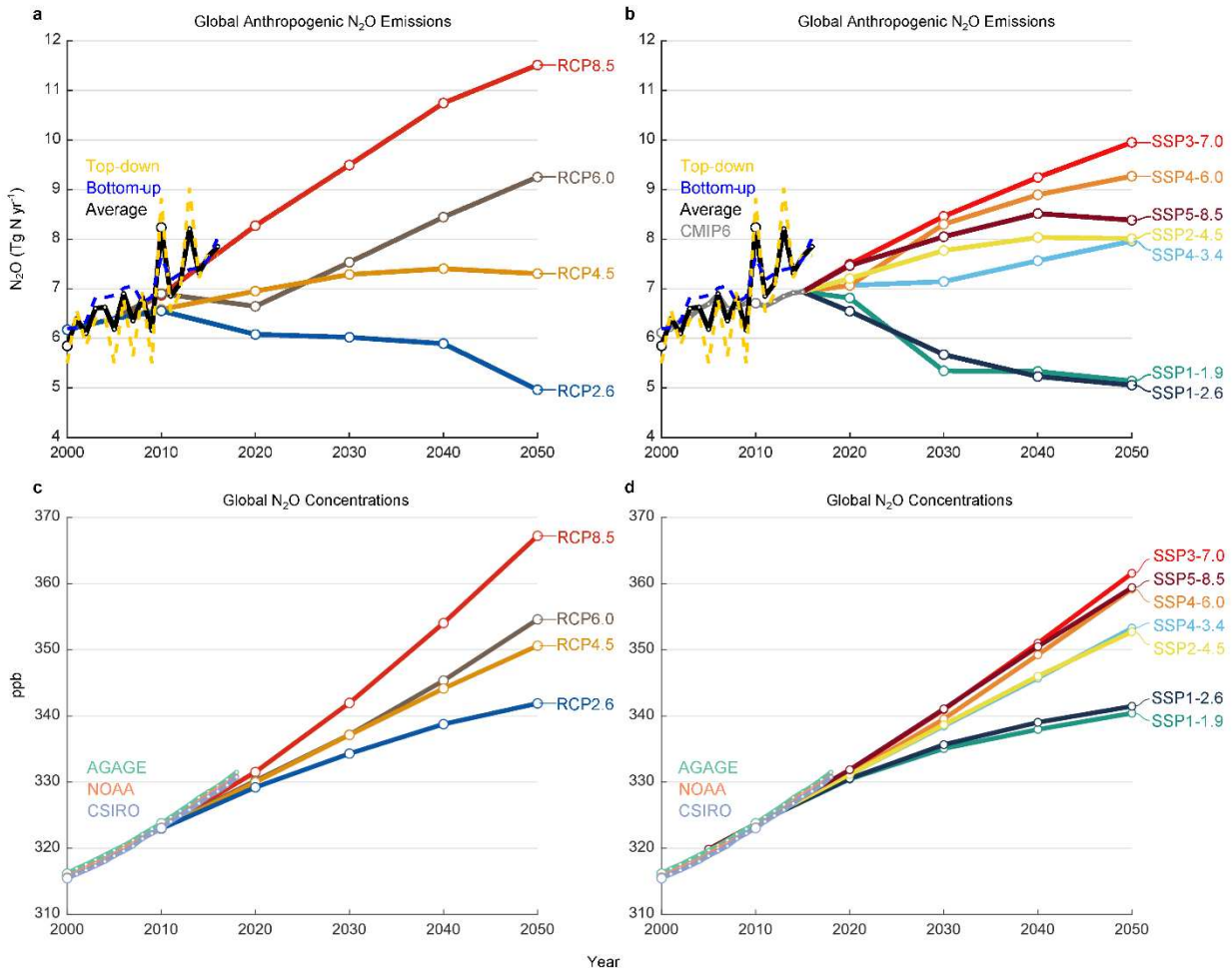
518
 519 **Fig. 2 Regional N₂O sources in the recent decade (2007–2016) over 11 regions.** *The Earth's*
 520 *ice-free land is partitioned into ten regions: North America (NA), South America (SA), Europe (EU),*
 521 *Middle East (MIDE), Africa (AF), Russia (RUS), East Asia (EAS), South Asia (SAS), Southeast Asia*
 522 *(SEA), and Oceania (OCE). In each subplot from left to right: emissions from five sub-sectors using BU*
 523 *approaches: natural fluxes without ocean (green), direct emissions of N additions in the agricultural*
 524 *sector (Agriculture, red), other direct anthropogenic sources (orange), indirect emissions from*
 525 *anthropogenic N additions (maroon), and perturbed fluxes from climate/CO₂/land cover change (brown);*
 526 *the sum of these five categories by BU approaches (blue), and the estimates by TD approaches (gold). BU*
 527 *and TD estimates of ocean emissions are shown at the bottom left (from bottom to top: 30°–90°N,*
 528 *30°S–30°N, and 90°–30°S). Error bars indicate the spread between the minimum and the maximum*
 529 *values. The center map shows the spatial distribution of 10-year average N₂O emissions from land and*
 530 *ocean based on the land and ocean models. Per capita N₂O emission (kg N capita⁻¹ yr⁻¹) during*
 531 *2007–2016 is shown in Supplementary Fig. 2.*
 532

533



534
 535 **Fig. 3 Ensembles of regional anthropogenic N_2O emissions over the 1980–2016 period.** *The*
 536 *bar chart in the center shows the accumulated changes in regional and global N_2O emissions during the*
 537 *study period. Error bars indicate the 95% confidence interval for the average of accumulated changes.*
 538 *The Mann-Kendall test was performed to examine a monotonic increasing or decreasing trend in the*
 539 *estimated ensemble N_2O emissions for each region and the globe during 1980–2016. The accumulated*
 540 *changes were calculated from the linear regressed annual change rate (Tg N yr⁻²) multiplied by 37 years.*
 541 *All regions except SEA show a significant increasing or decreasing trend in the estimated ensemble N_2O*
 542 *emissions during the study period (indicated by ** for each bar).*

543
 544



545
 546 **Fig. 4 Historical and projected global anthropogenic N_2O emissions and concentrations.**
 547 *Global anthropogenic N_2O emissions (a, b) and concentrations (c, d) compared to the four*
 548 *representative concentration pathways (RCPs) in the IPCC AR5 (a, c, ref. ²) and the new marker*
 549 *scenarios based on the Shared Socioeconomic Pathways (SSPs) used in CMIP6 (b, d, ref. ⁴¹).*
 550 *The historical data is represented as the mean of the BU and TD estimates of anthropogenic N_2O*
 551 *emissions, while the atmospheric concentration uses the three observation networks available,*
 552 *AGAGE, NOAA, and CSIRO. TD anthropogenic emissions were calculated by subtracting BU-*
 553 *derived natural fluxes. To aid the comparison, the four RCPs were shifted down so that the 2005*
 554 *value is equal to the 2000–2009 average of the mean of TD and BU estimates. The SSPs are*
 555 *harmonized³ to match the historical emissions used in CMIP6⁴² and Extended Data Fig. 10*
 556 *shows the unharmonized data.*

557

558

559

560 **Methods**

561 **Terminology.** This study provides an estimation of the global N₂O budget considering all
562 possible sources and all global change processes that can perturb the budget. A total of 18
563 sources and three sinks of N₂O are identified and grouped into six categories (Figure 1, Table 1):
564 1) Natural fluxes in absence of climate change and anthropogenic disturbances including Soil
565 emissions, Surface sink, Ocean emissions, Lightning and atmospheric production, and Natural
566 emission from inland waters, estuaries, coastal zones (inland and coastal waters), 2) Perturbed
567 fluxes from climate/CO₂/land cover change including CO₂ effect, Climate effect, Post-
568 deforestation pulse effect, and Long-term effect of reduced mature forest area, 3) Direct
569 emissions of N additions in the agricultural sector (Agriculture) including emissions from direct
570 application of synthetic N fertilizers and manure (henceforth Direct soil emissions), Manure left
571 on pasture, Manure management, and Aquaculture, 4) Indirect emissions from anthropogenic N
572 additions including atmospheric N deposition (NDEP) on land, atmospheric NDEP on ocean, and
573 effects of anthropogenic loads of reactive N in inland waters, estuaries, coastal zones, 5) Other
574 direct anthropogenic sources including Fossil fuel and industry, Waste and waste water, and
575 Biomass burning, and 6) Two estimates of stratospheric sinks obtained from atmospheric
576 chemistry transport models and observations, and one tropospheric sink (Table 1, Extended Data
577 Fig. 2).

578 For the purpose of compiling national GHG inventories for country reporting to the climate
579 convention, our anthropogenic N₂O emission categories are aligned with those used in UNFCCC
580 reporting and IPCC 2006 methodologies (Supplementary Table 14). We also provide the detailed
581 comparison of our methodology and quantification with the IPCC AR5 (see Supplementary
582 Section 4; Supplementary Table 15).

583 **Data synthesis.** We consider global N₂O emission from land and ocean consisting of natural
584 fluxes and anthropogenic emissions based on BU and TD approaches, however, the TD approach
585 cannot separate natural and anthropogenic sources.

586 ‘Natural soil baseline’ emissions were obtained from six terrestrial biosphere models
587 (NMIP¹⁶, Supplementary Tables 16–17) and provided here reflect a situation without
588 consideration of land use change (e.g., deforestation) and without consideration of indirect
589 anthropogenic effects via global change (i.e., climate, elevated CO₂, and atmospheric N
590 deposition). BU oceanic N₂O emissions were based on an inter-comparison of five global ocean
591 biogeochemistry models (Supplementary Table 18). The natural emission from ‘Inland water,
592 estuaries, coastal zones’ includes coastal upwelling⁵⁰ and inland and coastal waters that were
593 obtained from Yao et al.³⁶, Maavara et al.³⁵, and Lauerwald et al.⁵¹. Since the data (rivers,
594 reservoirs, and estuaries) provided by Maavara et al. and Lauerwald et al. are for the year 2000,
595 we assume that these values are constant during 1980–2016. Yao et al.³⁶ provided annual
596 riverine N₂O emissions using DLEM during the same period. Here, we averaged estimates from
597 Yao et al. with that from Maavara et al.³⁵. In addition, we estimated N₂O emissions from global
598 and regional reservoirs in the 2000s, and averaged their estimates with that from Maavara et al.³⁵
599 to represent emissions from reservoirs during 1980–2016. The estimate for global and regional
600 estuaries and lakes is still based on the long-term averaged values provided by Maavara et al.³⁵
601 and Lauerwald et al.⁵¹, respectively. We considered the riverine emissions in the year 1900 as
602 equivalent to the natural emission for the DLEM estimate assuming that the N load from land
603 was negligible in that period⁵². We quantified the contribution of natural sources to total
604 emission from reservoirs, lakes, and estuaries at 44% (36%–52%), with consideration of all N
605 inputs (i.e., inorganic, organic, dissolved, particulate forms). We combined the estimate from

606 lightning with that from atmospheric production into an integrated category ‘Lightning and
607 atmospheric production’. We make the simplification of considering the category ‘Lightning and
608 atmospheric production’ as purely natural, however, atmospheric production is affected to some
609 extent by anthropogenic activities through enhancing the concentrations of the reactive species
610 NH_2 and NO_2 . This category is in any case very small and the anthropogenic enhancement effect
611 is uncertain. Lightning produces NO_x , the median estimate of which is 5 Tg N yr^{-1} (ref. ⁵³). We
612 assumed an EF of 1% (ref. ⁵⁴) and a global estimate of $0.05 (0.02\text{--}0.09) \text{ Tg N yr}^{-1}$ from lightning.
613 Atmospheric production of N_2O results from the reaction of NH_2 with NO_2 (refs. ^{55,56}), N with
614 NO_2 , and oxidation of N_2 by $\text{O}(^1\text{D})$ ⁵⁷, all of which constitute an estimated source of $0.3 (0.2\text{--}1.1)$
615 Tg N yr^{-1} . The estimate of ‘Surface sink’ was obtained from Schlesinger⁵⁸ and Syakila et al.⁵⁹.

616 The anthropogenic sources include four sub-sectors:

617 **(a) Agriculture.** It consists of four components: ‘Direct soil emissions’, ‘Manure left on
618 pasture’, ‘Manure management’, and ‘Aquaculture’. Data for ‘Direct soil emissions’ were
619 obtained as the ensemble mean of N_2O emissions from an average of three inventories (EDGAR
620 v4.3.2, FAOSTAT, and GAINS), the SRNM/DLEM models, and the NMIP/DLEM models. The
621 statistical model SRNM only covers cropland N_2O emissions, the same as the NMIP. Thus, we
622 add the DLEM-based estimate of pasture N_2O emissions into the two estimates in cropland to
623 represent direct agricultural soil emissions (i.e., SRNM/DLEM or NMIP/DLEM). The ‘Manure
624 left on pasture’ and ‘Manure management’ emissions are the ensemble mean of EDGAR v4.3.2,
625 FAOSTAT, and GAINS databases. Global N flows (i.e., fish feed intake, fish harvest, and waste)
626 in freshwater and marine aquaculture were obtained from Beusen et al.³⁰ and Bouwman et al.^{60,61}
627 based on a nutrient budget model for the period 1980–2016. We then calculated global
628 aquaculture N_2O emissions through considering 1.8% loss of N waste in aquaculture, the same

629 EF used in Hu et al.⁶² and Macleod et al.³¹. The uncertainty range of the EF is from 0.5% (ref. ¹⁴)
630 to 5% (ref. ⁶³), the same range used in the UNEP report⁹. The ‘Aquaculture’ emission for the
631 period 2007–2016 was a synthesis data from Hu et al.⁶² in 2009, the FAO Report³¹ in 2013, and
632 our calculations. The estimate of aquaculture N₂O emission prior to 2009 was from our
633 calculations only.

634 The estimated direct emissions from agriculture have increased from 2.6 (1.8–4.1) Tg N yr⁻¹
635 in the 1980s to 3.8 (2.5–5.8) Tg N yr⁻¹ over the recent decade (2007–2016, Table 1).
636 Specifically, direct soil emission from the application of fertilizers is the major source and
637 increased at a rate of 0.27±0.01 Tg N yr⁻¹ per decade (P < 0.05; Table 1). Compared with the
638 three global inventories (FAOSTAT, EDGAR v4.3.2, and GAINS), the estimates from process-
639 based models (NMIP/DLEM^{15,16}) and a statistical model (SRNM)/DLEM^{15,17} exhibited a faster
640 increase (Extended Data Fig. 4a). Over the past four decades, we also found a small but
641 significant increase in emissions from livestock manure (i.e., manure left on pasture and manure
642 management) at a rate of 0.1±0.01 Tg N yr⁻¹ per decade (P < 0.05; Extended Data Fig. 4b-c).
643 Meanwhile, global aquaculture N₂O emissions increased 10-fold, however, this flux remains the
644 smallest term in the global budget (Extended Data Fig. 4d).

645 **(b) Other direct anthropogenic sources.** It includes ‘Fossil fuel and industry’, ‘Waste and
646 waste water’, and ‘Biomass burning’. Both ‘Fossil fuel and industry’ and ‘Waste and waste
647 water’ are the ensemble means of EDGAR v4.3.2 and GAINS databases. The ‘Biomass burning’
648 emission is the ensemble mean of FAOSTAT, DLEM, and GFED4s databases.

649 Emissions from a combination of fossil fuel and industry, waste and waste water, and biomass
650 burning increased from 1.8 (1.6–2.1) Tg N yr⁻¹ in the 1980s to 1.9 (1.6–2.3) Tg N yr⁻¹ over the
651 period of 2007–2016 (Table 1). The waste and waste water emission showed a continuous

652 increase at a rate of $0.04 \pm 0.01 \text{ Tg N yr}^{-1}$ per decade ($P < 0.05$) (Extended Data Fig. 5c).
653 Emissions from biomass burning, estimated based on three data sources (DLEM, GFED4s, and
654 FAOSTAT), slightly decreased at a rate of $-0.03 \pm 0.04 \text{ Tg N yr}^{-1}$ per decade ($P = 0.3$) since
655 the 1980s (Extended Data Fig. 5d). This item is largely affected by climate and land use
656 change^{64,65}. Of the three data sources, the DLEM estimate exhibited significant inter-annual
657 variability, especially during 1980–2000 when extreme fire events were detected in 1982, 1987,
658 1991, 1994, and 1998. The occurrences of these extreme fires were associated with El Niño-
659 Southern Oscillation (ENSO) events, especially in Indonesia (e.g., ‘Great Fire of Borneo’ in
660 1982)⁶⁶. Since 1997, N_2O emissions from fires estimated by DLEM, GFED4s, and FAOSTAT
661 were consistent in the inter-annual variability. All the three estimates showed a decreasing trend,
662 agreeing well with satellite-observed decrease of global burned area^{64,65}.

663 **(c) Indirect emissions from anthropogenic N additions.** Data were obtained from various
664 sources and considered N deposition on land and ocean (‘N deposition on land’ and ‘N
665 deposition on ocean’), as well as the N leaching and runoff from upstream (‘Inland and coastal
666 waters’). The emission from ‘N deposition on ocean’ was provided by Suntharalingam et al.⁶⁷,
667 while emission from ‘N deposition on land’ was the ensemble mean of an average of three
668 inventories: FAOSTAT/EDGAR v4.3.2, GAINS/EDGAR v4.3.2, and NMIP. FAOSTAT and
669 GAINS documented the sector ‘Indirect agricultural N_2O emissions’ by separating estimates
670 from N leaching or N deposition, while EDGAR v4.3.2 did not. Here, we treated ‘Indirect
671 agricultural N_2O emissions’ from EDGAR v4.3.2 as ‘Inland and coastal waters’ emissions for
672 data synthesis. Only EDGAR v4.3.2 provided an estimate of indirect emission from non-
673 agricultural sectors, while both FAOSTAT and GAINS, following the IPCC guidelines, provided
674 NH_3/NO_y volatilization from agricultural sectors. Here, we sum FAOSTAT or GAINS with

675 EDGAR v4.3.2 (i.e., FAOSTAT/EDGAR v4.3.2 or GAINS/EDGAR v4.3.2) to represent N
676 deposition induced soil emissions from both agricultural and non-agricultural sectors. The N₂O
677 emissions from ‘Inland and coastal waters’ consist of rivers, reservoirs, lakes, estuaries, and
678 coastal zone, which is the ensemble mean of an average of three inventories (EDGAR v4.3.2,
679 FAOSTAT, GAINS), and the mean of process-based models. The anthropogenic emission
680 estimated by Yao et al.³⁶ considered annual N inputs and other environmental factors (i.e.,
681 climate, elevated CO₂, and land cover change). For long-term average in rivers, reservoirs,
682 estuaries and lakes, we applied a mean of 56% (based on the ratio of anthropogenic to total N
683 additions from land) to calculate anthropogenic emissions. Seagrass, mangrove, saltmarsh and
684 intertidal N₂O emissions were undated from Murray et al⁶⁸. Coastal waters with low disturbance
685 generally either have low N₂O emissions or act as a sink for N₂O^{69,70}. Here, coastal zone
686 emissions were treated as anthropogenic emissions due to intensive human disturbances⁷¹.

687 N₂O emissions following transport of anthropogenic N additions via atmosphere and water
688 bodies increased from 1.1 (0.6–1.9) Tg N yr⁻¹ in the 1980s to 1.3 (0.7–2.2) Tg N yr⁻¹ during
689 2007–2016 (Table 1). The N₂O emissions from inland and coastal waters increased at a rate of
690 0.03±0.00 Tg N yr⁻¹ per decade (P < 0.05). Such an increase was reported by all the three
691 inventories (FAOSTAT, GAINS, and EDGAR v4.3.2) with FAOSTAT giving the largest
692 estimate. In contrast, the DLEM-based estimate presented a divergent trend: first increasing from
693 1980–1998 and then slightly decreasing thereafter (Extended Data Fig. 6a). Emissions from
694 atmospheric N deposition on oceans were relatively constant with a value of 0.1 (0.1–0.2) Tg N
695 yr⁻¹, while a large increase in emissions was found from atmospheric N deposition on land, with
696 0.06±0.01 Tg N yr⁻¹ per decade (P < 0.05) reported in the three estimates (FAOSTAT/EDGAR
697 v4.3.2, GAINS/EDGAR v4.3.2, and NMIP). The FAOSTAT agricultural source, together with

698 the EDGAR v4.3.2 industrial source, is consistent with NMIP estimates in the magnitude of N₂O
699 emissions, with the latter estimating a slightly slower increase from 2010 to 2016 (Extended
700 Data Fig. 6b).

701 **(d) Perturbed fluxes from climate/CO₂/land cover change.** Perturbed N₂O fluxes represent the
702 sum of the effects of climate, elevated atmospheric CO₂, and land cover change. The estimate of
703 climate and CO₂ effects on emissions was based on NMIP. The effect of land cover change on
704 N₂O dynamics includes the reduction due to ‘Long-term effect of reduced mature forest area’
705 and the emissions due to ‘Post-deforestation pulse effect’. The two estimates were based on the
706 book-keeping approach and the DLEM model simulation. The book-keeping method is
707 developed by Houghton et al.⁷² for accounting for carbon flows due to land use. In this study, an
708 observation dataset consisting of 18 tropical sites was collected to follow the book-keeping logic.
709 The dataset covers N₂O emissions from a reference mature forest and their nearby converted
710 pastures aged between one and 60 years. The average tropical forest N₂O emission rate of 1.974
711 kg N₂O-N ha⁻¹ yr⁻¹ was adopted as the baseline⁷³. Two logarithmic response curves of soil N₂O
712 emissions (normalized to the baseline) after deforestation were developed: $y = -0.31 \ln(x) +$
713 1.53 ($R^2 = 0.30$) and $y = -0.454 \ln(x) + 2.21$ ($R^2 = 0.09$). The first logarithmic function
714 uses data collected by a review analysis⁷⁴, based upon which the second one further considers
715 observations from Verchot et al.²¹ and Keller and Reiners⁷⁵. In the first function, x (unit: year)
716 indicates pasture age in years after deforestation and y (unitless; 0–1) indicates the ratio of
717 pasture N₂O emission over the N₂O emission from the nearby reference mature forest. In the
718 second function, x (unit: year) indicates secondary forest age and y (unitless; 0–1) indicates the
719 ratio of secondary forest N₂O emission over that of a reference mature forest. This form of the
720 response functions can effectively reproduce the short-lived increase in soil N₂O emissions after

721 initial forest clearing and the gradually declining emission rates of converted crops/pastures^{21,76}.
722 Using these two curves and the baseline, we kept track of the N₂O reduction of tropical forests
723 and the post-deforestation crop/pasture N₂O emissions at an annual time-scale. This book-
724 keeping method was applied to the two deforestation area datasets (Supplementary Text 2.8), so
725 we could investigate not only the difference caused by the two sets of land use data but also the
726 difference between this empirical method and the process-based model. For land conversion
727 from natural vegetation to croplands or pastures, DLEM uses a similar strategy to Houghton et
728 al.⁷² and McGuire et al.⁷⁷ to simulate its influences on carbon and N cycles. Moreover, through
729 using the sites of field observation from Davidson et al.²⁰ and Keller and Reiners⁷⁵, we estimated
730 N₂O emission from secondary tropical forests based on the algorithm: $y = 0.0084x + 0.2401$ (R^2
731 = 0.44). x (unit: year) indicates secondary forest age and y (unitless; 0–1) indicates the ratio of
732 secondary forest N₂O emission over that of a reference mature forest. The difference between
733 primary forests and secondary forests were subtracted from natural soil emissions simulated by
734 six terrestrial biosphere models in NMIP.

735 We calculated the ensemble of oceanic N₂O emission based on the BU approach (five ocean
736 biogeochemical models; Supplementary Table 18) and the TD approach (five estimates from
737 four inversion models; Supplementary Table 19), respectively. The atmospheric burden and its
738 rate of change during 1980–2016 were derived from mean maritime surface mixing ratios of
739 N₂O (refs. ^{78,79}) with a conversion factor of 4.79 Tg N/ppb (ref. ⁸⁰). Combining uncertainties in
740 measuring the mean surface mixing ratios⁷⁸ and that of converting surface mixing ratios to a
741 global mean abundance⁸⁰, we estimate a ±1.4% uncertainty in the burden. Annual change in
742 atmospheric abundance is calculated from the combined NOAA and AGAGE record of surface
743 N₂O and uncertainty is taken from the IPCC AR5 (ref. ²). There shows an agreement of the

744 stratospheric loss from atmospheric chemistry transport models (TD modeled chemical sink^{18,81})
745 and from satellite observations with a photolysis model (observed photochemical sink¹), which
746 differ only by ~ 1 Tg N yr⁻¹. The satellite-based lifetime, 116 ± 9 years, gives an overall
747 uncertainty in the annual loss of $\pm 8\%$. The tropospheric loss of N₂O from reaction with O(¹D) is
748 included in observed atmospheric chemical sink (Table 1) and is small ($\sim 1\%$ of the stratospheric
749 sink) with an estimated range of 0.1 to 0.2 Tg N yr⁻¹.

750 **Comparison with the IPCC guidelines.** The IPCC has provided guidance to quantify N₂O
751 emissions, which is widely used in emission inventories for reporting to the UNFCCC. Over time
752 the recommended approaches have changed, which is critical for estimating emissions from
753 agricultural soils, the largest emission source. Previous global N₂O assessments^{52,82,83} based on
754 the IPCC 1996 guidelines⁸⁴ attributed about 6.3 Tg N yr⁻¹ to the agricultural sector, including
755 both direct and indirect emissions. This estimate is significantly larger than our results (Fig. 1;
756 Table 1) derived from multiple methods, and is also larger than the most recent estimates from
757 global inventories (EDGAR v4.3.2, FAOSTAT, and GAINS) that are based on the IPCC 2006
758 guidelines¹⁴. The main reason is that indirect emissions from leaching and groundwater were
759 overestimated in previous studies⁸⁵. Correspondingly, projections of atmospheric N₂O
760 concentrations based on these overestimated emissions⁸² led to biased estimates. For example,
761 Mosier and Kroeze⁸² expected atmospheric N₂O concentrations to be 340–350 ppb in the year
762 2020, instead of 333 ppb⁵ as observed. Recently, the 2019 Refinement to the 2006 IPCC
763 Guidelines for National Greenhouse Gas Inventories has been published. It adopts the same
764 approach for N application on soils, but considers impacts of different climate regimes. The new
765 guidelines, based on a wealth of new scientific literature, proposed much smaller emissions from
766 grazing animals by a factor of 5–7. Preliminary calculations we have made indicate that global

767 soil emissions based on these new guidelines may decrease by 20%–25%. Integrating estimates
768 relying on the IPCC methodology with estimates by process-based models provides for a more
769 balanced assessment in this paper. We also added information from assessments^{86,87} that derived
770 agricultural emissions as the difference between atmospheric terms and other emissions like
771 combustion, industry and nature, and they gave comparable magnitudes (4.3–5.8 Tg N yr⁻¹) to
772 our bottom-up results.

773 **Uncertainty.** Current data analysis and synthesis of long-term N₂O fluxes are based on a wide
774 variety of TD and BU methods. TD approaches, consisting of four inversion frameworks⁸⁸⁻⁹¹,
775 provide a wide range of estimates largely due to systematic errors in the modelled atmospheric
776 transport and stratospheric loss of N₂O. In addition, the emissions from TD analyses are
777 dependent on the magnitude and distribution of the prior flux estimates to an extent that is
778 strongly determined by the number of atmospheric N₂O measurements¹⁸. Inversions are
779 generally not well constrained (and thus rely heavily on a priori estimates) in Africa, Southeast
780 Asia, southern South America, and over the oceans, owing to the paucity of observations in these
781 regions. The improvement of atmospheric transport models, more accurate priors, and more
782 atmospheric N₂O measurements would reduce uncertainty in further TD estimates, particularly
783 for ocean and regional emissions.

784 BU approaches are subject to uncertainties in various sources from land¹⁶ and oceans³². For
785 process-based models (e.g. NMIP and ocean biogeochemical models), the uncertainty is
786 associated with differences in model configuration as well as process parameterization^{16,32}. The
787 uncertainty of estimates from NMIP could be reduced in multiple ways¹⁶. First, the six models in
788 NMIP exhibited different spatial and temporal patterns of N₂O emissions even though they used
789 the same forcings. Although these models have considered essential biogeochemical processes in

790 soils (e.g., biological N fixation, nitrification/denitrification, mineralization/immobilization,
791 etc.)⁹², some missing processes such as freeze-thaw cycles and ecosystem disturbances should be
792 included in terrestrial biosphere models to reduce uncertainties. Second, the quality of input
793 datasets, specifically the amount and timing of N application, and spatial and temporal changes
794 in distribution of natural vegetation and agricultural land, is critical for accurately simulating soil
795 N₂O emissions. Third, national and global N₂O flux measurement networks¹⁷ could be used to
796 validate model performance and constrain large-scale model simulations. Data assimilation
797 techniques could be utilized to improve model accuracy.

798 Current remaining uncertainty in global ocean model estimates of N₂O emission includes the
799 contribution of N₂O flux derived from the tropical oceanic low oxygen zones (e.g., the Eastern
800 Equatorial Pacific, the northern Indian ocean) relative to the global ocean. These low oxygen
801 zones are predominantly influenced by high yield N₂O formation processes (e.g., denitrification
802 and enhanced nitrification). Regional observation-based assessments have also suggested that
803 these regions may produce more N₂O than is simulated by the models³². The current generation
804 of global ocean biogeochemistry models are not sufficiently accurate to represent the high N₂O
805 production processes in low-oxygen zones, and their associated variability (see refs. ^{34,93,94} for
806 more detail). Thus, precisely representing the local ocean circulation and associated
807 biogeochemical fluxes of these regions could further reduce the uncertainty in estimates of
808 global and regional oceanic N₂O emissions.

809 Regardless of the tier approach used, GHG inventories for agriculture suffer from high
810 uncertainty in the underlying agriculture and rural data and statistics used as input, including
811 statistics on fertilizer use, livestock manure availability, storage and applications, and nutrient,
812 crop and soils management. For instance, animal waste management is an uncertain aspect, since

813 much of the manure is either not used, or employed as a fuel or building material, or may be
814 discharged directly to surface water^{95,96}, with important repercussions for the calculated
815 emissions. Furthermore, GHG inventories using default EFs show large uncertainties at local to
816 global scales, especially for agricultural N₂O emissions, due to the poorly captured dependence
817 of EFs on spatial diversity in climate, management, and soil physical and biochemical
818 conditions^{2,22}. It is well known, for example from the IPCC guidelines, that higher-tier GHG
819 inventories may provide more reasonable estimates by using the alternative EFs that are
820 disaggregated by environmental factors and management-related factors⁹⁷. A large range of EFs
821 have been used to estimate aquaculture N₂O emissions^{31,39,62,86} and long-term estimates of N
822 flows in freshwater and marine aquaculture are scarce³⁰. Uncertainty also remains in several N₂O
823 sources that have not yet been fully understood or quantified. To date, robust estimates of N₂O
824 emissions from global peatland degradation are still lacking, although we have accounted for
825 N₂O emissions due to the drainage of organic soils (histosols) obtained from FAOSTAT and
826 GAINS databases^{28,43}. Recent evidence shows that permafrost thawing⁹⁸ and the freeze-thaw
827 cycle⁹⁹ contribute to increasing N₂O emissions, which, however, have not been well established
828 in the current estimates of the global N₂O budget.

829 **Statistics.** Through using the Mann-Kendall test in R-3.4.4, we checked the significance of
830 trends in annual N₂O emissions from each sub-sector based on the BU approach.

831 **References**

832

- 833 50 Nevison, C. D., Lueker, T. J. & Weiss, R. F. Quantifying the nitrous oxide source from
834 coastal upwelling. *Global Biogeochemical Cycles* **18**, GB1018 (2004).
- 835 51 Lauerwald, R. *et al.* Natural lakes are a minor global source of N₂O to the atmosphere.
836 *Global Biogeochemical Cycles* **33**, 1564-1581 (2019).
- 837 52 Kroeze, C., Mosier, A. & Bouwman, L. Closing the global N₂O budget: a retrospective
838 analysis 1500–1994. *Global Biogeochemical Cycles* **13**, 1-8 (1999).

- 839 53 Schumann, U. & Huntrieser, H. The global lightning-induced nitrogen oxides source.
840 *Atmospheric Chemistry and Physics* **7**, 3823-3907 (2007).
- 841 54 De Klein, C. *et al.* N₂O emissions from managed soils, and CO₂ emissions from lime and
842 urea application. *IPCC Guidelines for National Greenhouse Gas Inventories, Prepared*
843 *by the National Greenhouse Gas Inventories Programme* **4**, 1-54 (2006).
- 844 55 Dentener, F. J. & Crutzen, P. J. A three-dimensional model of the global ammonia cycle.
845 *Journal of Atmospheric Chemistry* **19**, 331-369 (1994).
- 846 56 Röckmann, T., Kaiser, J., Crowley, J. N., Brenninkmeijer, C. A. & Crutzen, P. J. The
847 origin of the anomalous or "mass-independent" oxygen isotope fractionation in
848 tropospheric N₂O. *Geophysical Research Letters* **28**, 503-506 (2001).
- 849 57 Kaiser, J. & Röckmann, T. Absence of isotope exchange in the reaction of N₂O+O(¹D)
850 and the global Δ¹⁷O budget of nitrous oxide. *Geophysical Research Letters* **32** (2005).
- 851 58 Schlesinger, W. H. An estimate of the global sink for nitrous oxide in soils. *Global*
852 *Change Biology* **19**, 2929-2931 (2013).
- 853 59 Syakila, A., Kroeze, C. & Slomp, C. P. Neglecting sinks for N₂O at the earth's surface:
854 does it matter? *Journal of Integrative Environmental Sciences* **7**, 79-87 (2010).
- 855 60 Bouwman, A. F. *et al.* Hindcasts and future projections of global inland and coastal
856 nitrogen and phosphorus loads due to finfish aquaculture. *Reviews in Fisheries Science*
857 **21**, 112-156 (2013).
- 858 61 Bouwman, A. F. *et al.* Global hindcasts and future projections of coastal nitrogen and
859 phosphorus loads due to shellfish and seaweed aquaculture. *Reviews in Fisheries Science*
860 **19**, 331-357 (2011).
- 861 62 Hu, Z., Lee, J. W., Chandran, K., Kim, S. & Khanal, S. K. Nitrous oxide (N₂O) emission
862 from aquaculture: a review. *Environmental science technology* **46**, 6470-6480 (2012).
- 863 63 Williams, J. & Crutzen, P. J. Nitrous oxide from aquaculture. *Nature Geoscience* **3**, 143
864 (2010).
- 865 64 Andela, N. *et al.* A human-driven decline in global burned area. *Science* **356**, 1356-1362
866 (2017).
- 867 65 Yang, J. *et al.* Spatial and temporal patterns of global burned area in response to
868 anthropogenic and environmental factors: Reconstructing global fire history for the 20th
869 and early 21st centuries. *Journal of Geophysical Research: Biogeosciences* **119**, 249-263
870 (2014).
- 871 66 Dennis, R. A review of fire projects in Indonesia (1982-1998). *Cifor* (1999).
- 872 67 Suntharalingam, P. *et al.* Quantifying the impact of anthropogenic nitrogen deposition on
873 oceanic nitrous oxide. *Geophysical Research Letters* **39**, L07605 (2012).
- 874 68 Murray, R. H., Erler, D. V. & Eyre, B. D. Nitrous oxide fluxes in estuarine environments:
875 response to global change. *Global Change Biology* **21**, 3219-3245 (2015).
- 876 69 Erler, D. V. *et al.* Applying cavity ring - down spectroscopy for the measurement of
877 dissolved nitrous oxide concentrations and bulk nitrogen isotopic composition in aquatic
878 systems: Correcting for interferences and field application. *Limnology and*
879 *Oceanography: Methods* **13**, 391-401 (2015).
- 880 70 Murray, R., Erler, D., Rosentreter, J. & Eyre, B. Seasonal and spatial N₂O concentrations
881 and emissions in three tropical estuaries. *Marine Chemistry* **221**, 103779 (2020).
- 882 71 Vernberg, F. J. & Vernberg, W. B. *The coastal zone: past, present, and future*. Univ of
883 South Carolina Press (2001).

884 72 Houghton, R. *et al.* Changes in the Carbon Content of Terrestrial Biota and Soils between
885 1860 and 1980: A Net Release of CO₂ to the Atmosphere. *Ecological monographs* **53**,
886 235-262 (1983).

887 73 Davidson, E. A. The contribution of manure and fertilizer nitrogen to atmospheric nitrous
888 oxide since 1860. *Nature Geoscience* **2**, 659-662 (2009).

889 74 van Lent, J., Hergoualc'h, K. & Verchot, L. V. Reviews and syntheses: Soil N₂O and NO
890 emissions from land use and land-use change in the tropics and subtropics: a meta-
891 analysis. *Biogeosciences* **12**, 7299-7313 (2015).

892 75 Keller, M. & Reiners, W. A. Soil-atmosphere exchange of nitrous oxide, nitric oxide, and
893 methane under secondary succession of pasture to forest in the Atlantic lowlands of Costa
894 Rica. *Global Biogeochemical Cycles* **8**, 399-409 (1994).

895 76 Melillo, J. M. *et al.* Nitrous oxide emissions from forests and pastures of various ages in
896 the Brazilian Amazon. *Journal of Geophysical Research: Atmospheres* **106**, 34179-34188
897 (2001).

898 77 McGuire, A. *et al.* Carbon balance of the terrestrial biosphere in the twentieth century:
899 Analyses of CO₂, climate and land use effects with four process-based ecosystem models.
900 *Global Biogeochemical Cycles* **15**, 183-206 (2001).

901 78 Dlugokencky, E., Steele, L., Lang, P. & Masarie, K. The growth rate and distribution of
902 atmospheric methane. *Journal of Geophysical Research: Atmospheres* **99**, 17021-17043
903 (1994).

904 79 Prather, M. *et al.* Annex II: Climate system scenario tables. *Cambridge, United Kingdom
905 and New York, NY, USA* (2013).

906 80 Prather, M. J., Holmes, C. D. & Hsu, J. Reactive greenhouse gas scenarios: Systematic
907 exploration of uncertainties and the role of atmospheric chemistry. *Geophysical Research
908 Letters* **39**, L09803 (2012).

909 81 Prather, M. J. & Hsu, J. Coupling of Nitrous Oxide and Methane by Global Atmospheric
910 Chemistry. *Science* **330**, 952-954 (2010).

911 82 Mosier, A. & Kroeze, C. Potential impact on the global atmospheric N₂O budget of the
912 increased nitrogen input required to meet future global food demands. *Chemosphere-
913 Global Change Science* **2**, 465-473 (2000).

914 83 Mosier, A. *et al.* Closing the global N₂O budget: nitrous oxide emissions through the
915 agricultural nitrogen cycle. *Nutrient cycling in Agroecosystems* **52**, 225-248 (1998).

916 84 IPCC. Revised 1996 IPCC guidelines for national greenhouse gas inventories. *Hayama,
917 Japan* (1997).

918 85 Nevison, C. in IPCC, Background Papers: IPCC Expert Meetings on Good Practice
919 Guidance and Uncertainty Management in National Greenhouse Gas Inventories. *IPCC
920 National Greenhouse Gas Inventories Programme, Technical Support Unit*. 381-397
921 (2000).

922 86 Crutzen, P. J., Mosier, A. R., Smith, K. A. & Winiwarter, W. N₂O release from agro-
923 biofuel production negates global warming reduction by replacing fossil fuels.
924 *Atmospheric Chemistry and Physics* **8**, 389-395 (2008).

925 87 Smith, K. A., Mosier, A. R., Crutzen, P. J. & Winiwarter, W. The role of N₂O derived
926 from crop-based biofuels, and from agriculture in general, in Earth's climate.
927 *Philosophical Transactions of the Royal Society of London B: Biological Sciences* **367**,
928 1169-1174 (2012).

929 88 Thompson, R. L. *et al.* Nitrous oxide emissions 1999 to 2009 from a global atmospheric
930 inversion. *Atmospheric Chemistry and Physics* **14**, 1801-1817 (2014).

931 89 Wells, K. C. *et al.* Simulation of atmospheric N₂O with GEOS-Chem and its adjoint:
932 evaluation of observational constraints. *Geoscience Model Development* **8**, 3179-3198
933 (2015).

934 90 Wilson, C., Chipperfield, M., Gloor, M. & Chevallier, F. Development of a variational
935 flux inversion system (INVICAT v1. 0) using the TOMCAT chemical transport model.
936 *Geoscientific Model Development* **7**, 2485-2500 (2014).

937 91 Patra, P. K. *et al.* Improved Chemical Tracer Simulation by MIROC4. 0-based
938 Atmospheric Chemistry-Transport Model (MIROC4-ACTM). *Sola* **14**, 91-96 (2018).

939 92 Tian, H. Q. *et al.* The Global N₂O Model Intercomparison Project. *Bulletin of the*
940 *American Meteorological Society* **99**, 1231-1252 (2018).

941 93 Suntharalingam, P. *et al.* Anthropogenic nitrogen inputs and impacts on oceanic N₂O
942 fluxes in the northern Indian Ocean: The need for an integrated observation and
943 modelling approach. *Deep Sea Research Part II: Topical Studies in Oceanography* **166**,
944 104-113 (2019).

945 94 Battaglia, G. & Joos, F. Marine N₂O Emissions From Nitrification and Denitrification
946 Constrained by Modern Observations and Projected in Multimillennial Global Warming
947 Simulations. *Global Biogeochemical Cycles* **32**, 92-121 (2018).

948 95 Galloway, J. *et al.* The impact of animal production systems on the nitrogen cycle. Vol.
949 1, *Island Press* (2010).

950 96 Steinfeld, H., Mooney, H. A., Schneider, F. & Neville, L. E. Livestock in a changing
951 landscape, volume 1: drivers, consequences, and responses. Vol. 1, *Island Press* (2013).

952 97 IPCC. 2019 Refinement to the 2006 IPCC Guidelines for National Greenhouse Gas
953 Inventories. *Hayama, Japan* (2019).

954 98 Elberling, B., Christiansen, H. H. & Hansen, B. U. High nitrous oxide production from
955 thawing permafrost. *Nature Geoscience* **3**, 332-335 (2010).

956 99 Wagner-Riddle, C. *et al.* Globally important nitrous oxide emissions from croplands
957 induced by freeze–thaw cycles. *Nature Geoscience* **10**, 279-283 (2017).

958 100 Suntharalingam, P. *et al.* Estimates of Oceanic Nitrous-oxide Emissions from Global
959 Biogeochemistry Models. *American Geophysical Union, Fall Meeting 2018* (2018).

960 101 Janssens-Maenhout, G. *et al.* EDGAR v4.3.2 Global Atlas of the three major greenhouse
961 gas emissions for the period 1970–2012. *Earth System Science Data* **11**, 959-1002
962 (2019).

963 102 Tubiello, F. *et al.* Estimating greenhouse gas emissions in agriculture: a manual to
964 address data requirements for developing countries. *FAO, Rome* (2015).

965 103 Van Der Werf, G. R. *et al.* Global fire emissions estimates during 1997-2016. *Earth*
966 *System Science Data* **9**, 697-720 (2017).

967 104 Dentener, F. Global maps of atmospheric nitrogen deposition, 1860, 1993, and 2050.
968 *Data set. Available on-line (<http://daac.ornl.gov/>) from Oak Ridge National Laboratory*
969 *Distributed Active Archive Center, Oak Ridge, TN, USA* (2006).

970 105 Riahi, K. *et al.* The Shared Socioeconomic Pathways and their energy, land use, and
971 greenhouse gas emissions implications: An overview. *Global Environmental Change* **42**,
972 153-168 (2017).

973
974 **Data availability**

975 The relevant datasets of this study are archived in the box site of International Center for Climate
976 and Global Change Research at Auburn University (<https://auburn.box.com/>). Source data for
977 Figs. 1–4, Table 1, Extended Figs. 1–10 and Supplementary Information are provided with the
978 paper. Additional description on data availability for atmospheric N₂O observations from
979 NOAA, AGAGE and CSIRO networks is provided in the Supplementary Information. The data
980 presented here are made available in the belief that their dissemination will lead to greater
981 understanding and new scientific insights on the global and regional N₂O budgets and changes to
982 it, and helping to reduce the uncertainties. As data are the result of initial processing to fit to the
983 purpose of this publication, typically a wealth of underlying information is with the original data
984 providers. Researchers interested to use results made available in the repository are encouraged,
985 as good practice, to take advantage of underlying information by contacting the original data
986 providers. If such a contact develops into a more intensive scientific discussion, further
987 involvement including co-authorship should be considered.

988

989 **Code availability**

990 The relevant codes of this study are archived in the box site of International Center for Climate
991 and Global Change Research at Auburn University (<https://auburn.box.com/>).

992

993 **Acknowledgements**

994 This paper is the result of a collaborative international effort under the umbrella of the Global
995 Carbon Project (a project of Future Earth and a research partner of the World Climate Research
996 Programme) and International Nitrogen Initiative. This research was made possible partly by
997 Andrew Carnegie Fellowship Award no. G-F-19-56910; NSF grant nos. 1903722, 1243232 and
998 1922687; NASA grant nos. NNX14AO73G, NNX10AU06G, NNX11AD47G and
999 NNX14AF93G; NOAA grant nos. NA16NOS4780207 and NA16NOS4780204; National Key R
1000 & D Program of China (grant nos. 2017YFA0604702 and 2018YFA0606001), National Natural
1001 Science Foundation of China (Grant no. 41961124006), CAS grants (KFJ-STSZDTP-0;
1002 SKLURE2017-1-6), and OUC-AU Joint Center Program. Additional funding support includes:
1003 E.T.B, P.R., G.P.P., R.L.T., P.S. acknowledge funding support from VERIFY project (EC H2020
1004 grant no. 776810). P.S. also acknowledges funding from the EC H2020 grant No 641816
1005 (CRESCENDO); A.I. acknowledges funding support from JSPS KAKENHI grant (no.
1006 17H01867). G.B., F.J, and S.L. acknowledge support by Swiss National Science Foundation
1007 (#200020_172476) and by the EC H2020 grant no. 821003 (Project 4C) and no. 820989 (Project
1008 COMFORT). A.L. acknowledges support by DFG project SFB754/3. S.Z. acknowledges support
1009 by the EC H2020 grant no. 647204. K.C.W. and D.B.M. acknowledge support from NASA (IDS
1010 Grant #NNX17AK18G) and NOAA (Grant #NA13OAR4310086); P.A.R. acknowledges NASA
1011 Award NNX17AI74G, M.M. acknowledges support from the Scottish Government’s Rural and
1012 Environment Science and Analytical Services Division (RESAS) Environmental Change
1013 Programme (2016-2021); B.E. acknowledges the support from ARC Linkage Grants
1014 LP150100519 and LP190100271; M.P. acknowledges US Department of Energy, DE-
1015 SC0012536; Lawrence Livermore National Laboratory, B628407 and NASA MAP program,
1016 NNX13AL12G; S.B. was supported by the EC H2020 with the CRESCENDO project (grant no.
1017 641816) and by the COMFORT project (grant no. 820989). S.B. also acknowledges the support
1018 of the team in charge of the CNRM-CM climate model; F.Z. acknowledges the support from the

1019 National Natural Science Foundation of China (41671464). Supercomputing time was provided
1020 by the Météo-France/DSI supercomputing center. P.K.P. is partly supported by Environment
1021 Research and Technology Development Fund (#2-1802) of the Ministry of the Environment,
1022 Japan. R.L. acknowledges support from the French state aid managed by the ANR under the
1023 "Investissements d'avenir" programme with the reference ANR-16-CONV-0003. NOAA ground-
1024 based observations of atmospheric N₂O are supported by NOAA's Climate Program Office under
1025 the Atmospheric Chemistry Carbon Cycle and Climate (AC4) theme. The AGAGE stations
1026 measuring N₂O are supported by NASA (USA) grants NNX16AC98G to MIT, and
1027 NNX16AC97G and NNX16AC96G to SIO, and by BEIS (UK) for Mace Head, NOAA (USA)
1028 for Barbados, and CSIRO and BoM (Australia) for Cape Grim. We also thank Dr. Steve Frohling
1029 and two anonymous reviewers for constructive comments and suggestions that have helped
1030 improve this paper. The statements made and views expressed are solely the responsibility of the
1031 authors.
1032

1033 **Author contributions**

1034 Author contributions. H.T., R.L.T., J.G.C. and R.B.J. designed and coordinated the study. H.T.,
1035 R.X., J.G.C., R.L.T., W.W., P.S., E.A.D., P.C., R.B.J., G.J.M., M.J.P., N.P., S.P., P.R., H.S.,
1036 F.N.T., S.Z., F.Z., B.F. and G.P. conducted data analysis, synthesis and wrote the paper. R.L.T.
1037 led atmospheric inversions teaming with M.P.C., T.M., D.B.M., P.K.P., K.C.W., and C.W.; H.T.
1038 led land biosphere modeling teaming with P.C., H.S., S.Z., A.A., F.J., J.C., S.R.S.D., A.I., W.L.,
1039 S.L., S.O., N.V., E.A.D., S.D. and W. Li; P.S. led ocean biogeochemical modeling teaming with
1040 G.B., L.B., S.B., E.T.B., F.J. and A.L.; P.R. led inland water and coastal modeling and synthesis
1041 teaming with B.D.E., G.G.L., R.L., T.M., P.A.R., H.T. and Y.Y.; A.F.B., J.W., M.M. provided
1042 data of N₂O flux in aquaculture. G.R.W. and J.Y. provided data of N₂O emissions from biomass
1043 burning. F.Z. provided cropland N₂O flux data from a statistical model and field observations.
1044 G.J.M., F.N.T. and W.W. provided N₂O inventory data. M.J.P. and D.J.R. provided data of
1045 stratospheric and tropospheric sinks. G.P.P. provided RCP and SSP scenarios data and analysis.
1046 B.H., E.D. and J.E. provided a global N₂O monitoring dataset of NOAA/ESRL GMD. R.P. and
1047 R.W. provided a global N₂O monitoring dataset of AGAGE stations. P.K. provided a global N₂O
1048 monitoring dataset of CSIRO. All coauthors reviewed and commented on the manuscript.
1049

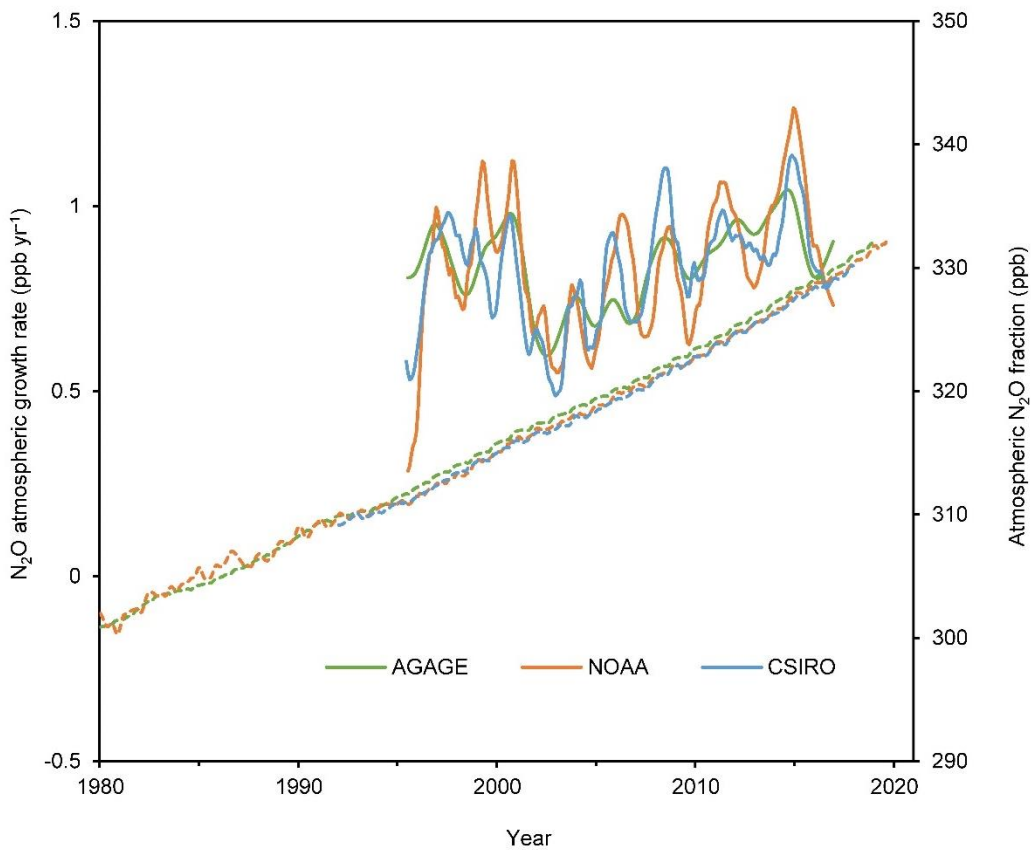
1050 **Competing interests: The authors declare no competing interests.**

1051
1052 **Additional information**

1053
1054 **Supplementary information is available for this paper at <https://>**

1055
1056 **Correspondence and requests for materials should be addressed to H.T.**

1057 tianhan@auburn.edu

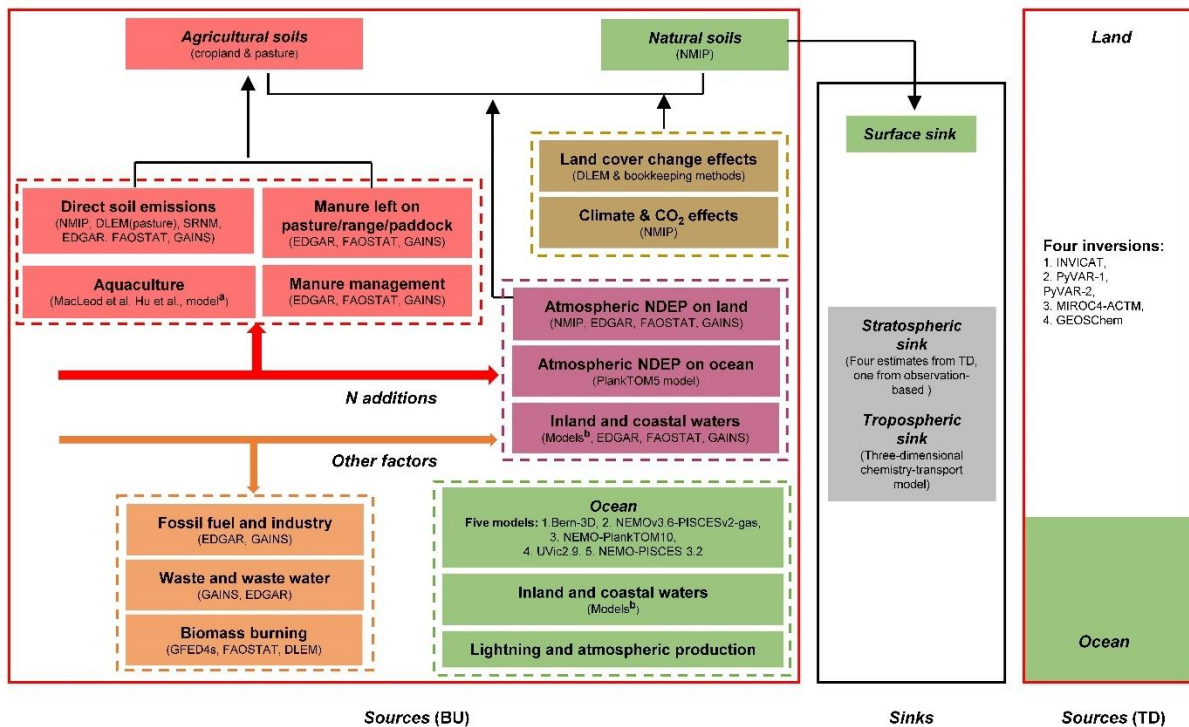


1058

1059 **Extended Data Fig. 1 Global mean growth rates and atmospheric concentration of N₂O.**

1060 Global mean growth rates (solid lines, during 1995–2017) and atmospheric N₂O concentration
 1061 (dashed lines, during 1980–2017) are from the AGAGE⁶ (green), NOAA⁵ (orange), and CSIRO
 1062 (blue) networks. Global mean growth rates were calculated with annual time steps and are shown
 1063 as 12-month moving averages. Growth rates are not calculated prior to 1995 due to insufficient
 1064 data and higher uncertainties on the measurements.

1065

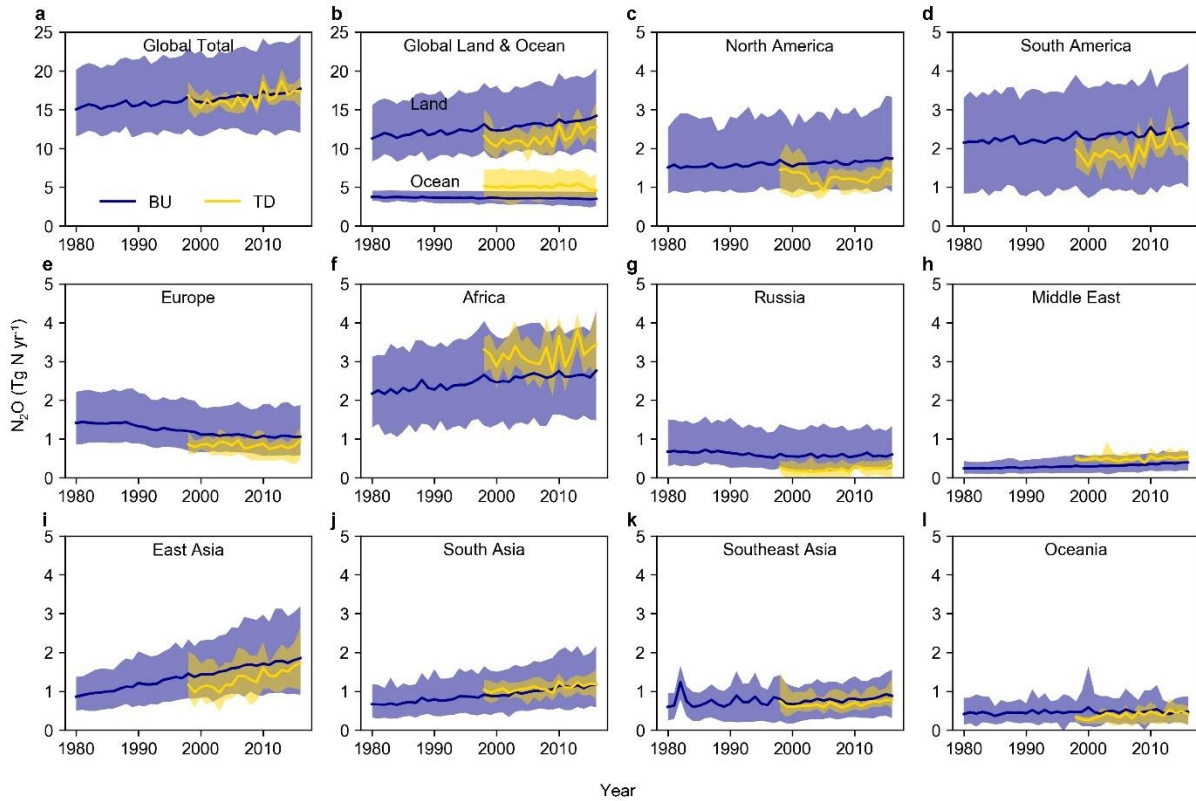


1066

1067 **Extended Data Fig. 2 The methodology for data synthesis of global N₂O budget.** BU and TD
 1068 represent bottom-up and top-down methods, respectively. The color codes are the same as that
 1069 used in Table 1 and Figs. 1–3. We utilize both approaches, including 22 BU and five TD
 1070 estimates of N₂O fluxes from land and oceans. For sources estimated by BU, we include six
 1071 process-based terrestrial biosphere modeling studies¹⁶; five process-based ocean biogeochemical
 1072 models¹⁰⁰; one nutrient budget model^{30,60,61}; five inland water modeling studies^{35,36,50,51,68}; one
 1073 statistical model SRNM based on spatial extrapolation of field measurements¹⁷; and four GHG
 1074 inventories: EDGAR v4.3.2¹⁰¹, FAOSTAT¹⁰², GAINS⁴³, and GFED4s¹⁰³. In addition, previous
 1075 literatures regarding estimates of ‘Surface sink’^{58,73}, ‘Lightning’^{53,54}, ‘Atmospheric
 1076 production’^{56,57,104}, ‘Aquaculture’^{31,62}, and model-based ‘Tropospheric sink’⁸¹ and observed
 1077 ‘Stratospheric sink’¹ are included in the current synthesis. ^aMacLeod et al.³¹ and Hu et al.⁶²
 1078 provide global aquaculture N₂O emissions in 2013 and in 2009, respectively; and the nutrient
 1079 budget model^{30,60,61} provides N flows in global freshwater and marine aquaculture over the
 1080 period 1980–2016. ^bModel-based estimates of N₂O emissions from ‘Inland and coastal waters’
 1081 include rivers and reservoirs^{35,36}, lakes⁵¹, estuaries³⁵, coastal zones (i.e., seagrasses, mangroves,
 1082 saltmarsh and intertidal saltmarsh)⁶⁸, and coastal upwelling⁵⁰.

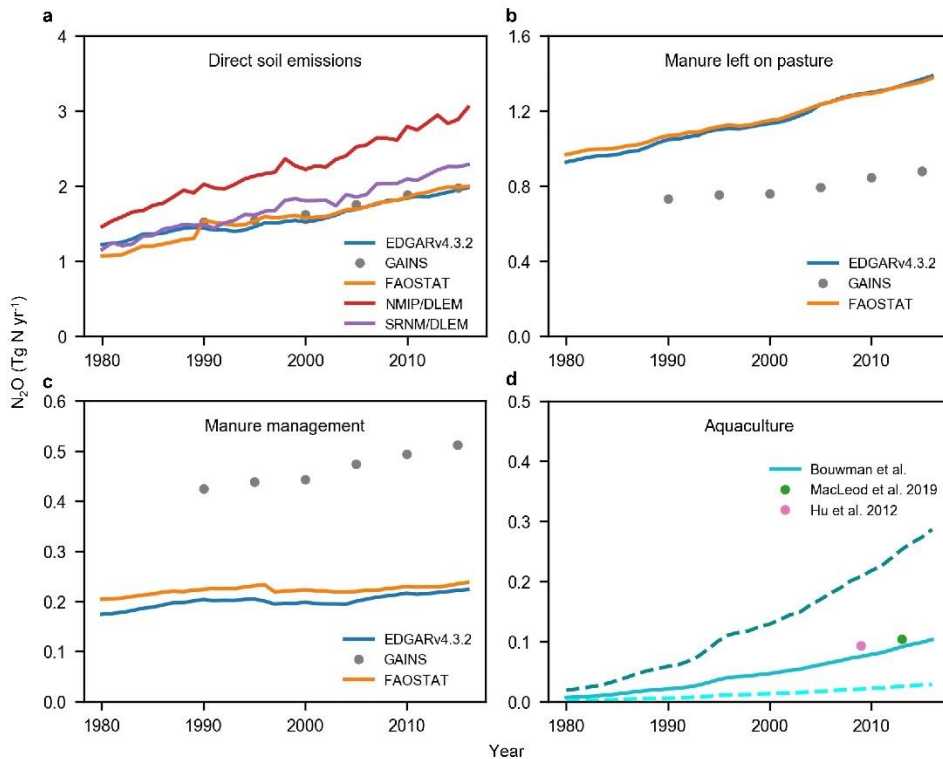
1083

1084

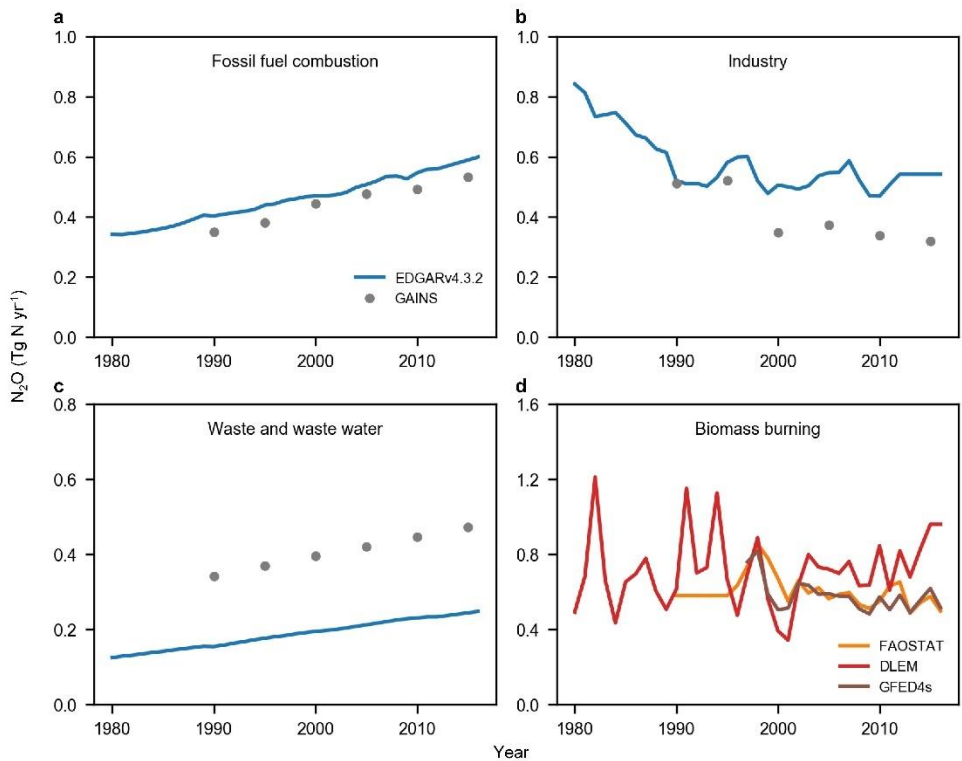


1085
 1086
 1087
 1088
 1089
 1090
 1091

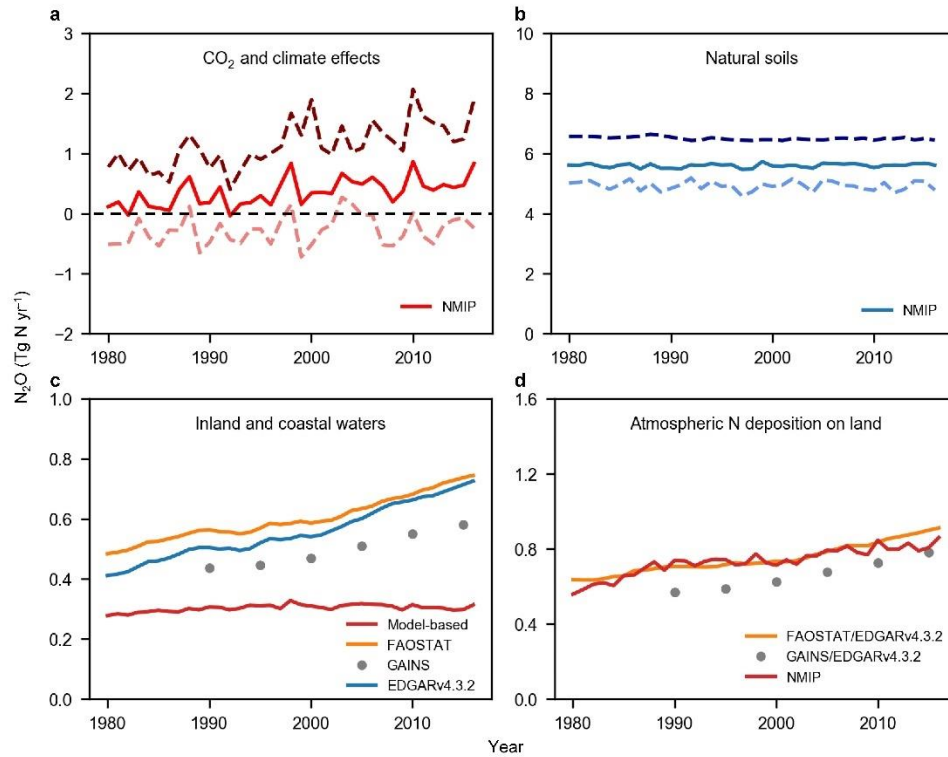
Extended Data Fig. 3 Comparison of annual total N₂O emissions at global and regional scales estimated by BU and TD approaches. The blue lines represent the mean N₂O emission from BU methods and the shaded areas show minimum and maximum estimates; The gold lines represent the mean N₂O emission from TD methods and the shaded areas show minimum and maximum estimates.



1092
 1093 **Extended Data Fig. 4 Global agricultural N₂O emissions.** **a**, Direct emission from agricultural
 1094 soils associated with mineral fertilizer, manure and crop residue inputs, and cultivation of
 1095 organic soils based on EDGAR v4.3.2, GAINS, FAOSTAT, NMIP/DLEM, and SRNM/DLEM
 1096 estimates. NMIP/DLEM or SRNM/DLEM means the combination of N₂O emission by NMIP or
 1097 SRNM from croplands with N₂O emission from intensively managed grassland (pasture) by
 1098 DLEM. **b**, Direct emission from the global total area under permanent meadows and pasture, due
 1099 to manure N deposition (left on pasture) based on EDGAR v4.3.2, FAOSTAT, and GAINS
 1100 estimates. **c**, Emission from manure management based on FAOSTAT, GAINS, and EDGAR
 1101 v4.3.2. **d**, Aquaculture N₂O emission based on a nutrient budget model³⁰, MacLeod et al.³¹, and
 1102 Hu et al.⁶²; the solid line represents the ‘best estimate’ that is the product of EF (1.8%) and N
 1103 waste from aquaculture provided by the nutrient budget model; the dashed lines represent the
 1104 minimum and maximum values.
 1105

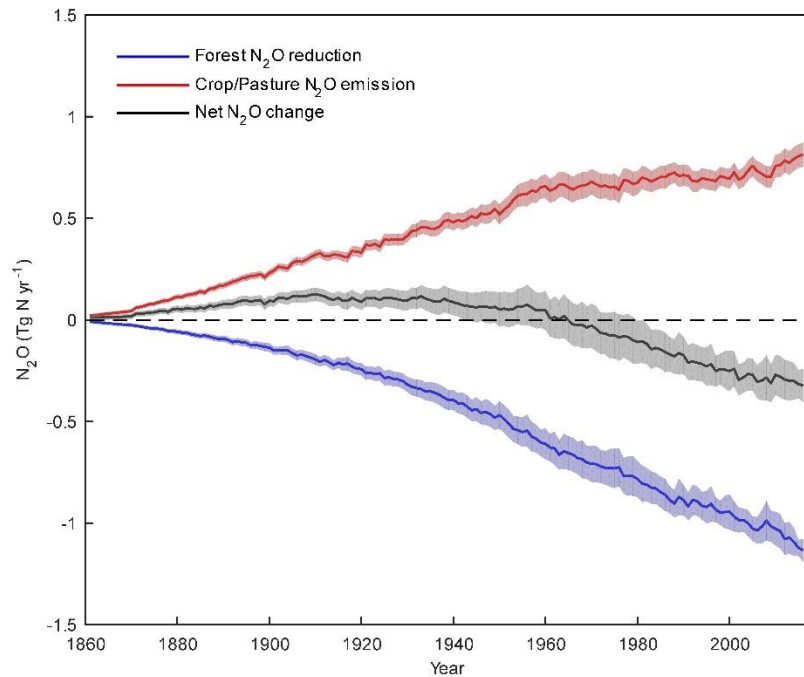


1106
 1107 **Extended Data Fig. 5 Global N₂O emission from other direct anthropogenic sources. a,**
 1108 **Emission from fossil fuel combustion based on EDGAR v4.3.2 and GAINS estimates. b,**
 1109 **Emission from industry based on EDGAR v4.3.2 and GAINS estimates. c, Emission from waste**
 1110 **and waste water based on EDGAR v4.3.2 and GAINS estimates. d, Emission from biomass**
 1111 **burning based on FAOSTAT, DLEM, and GFED4s estimates.**
 1112

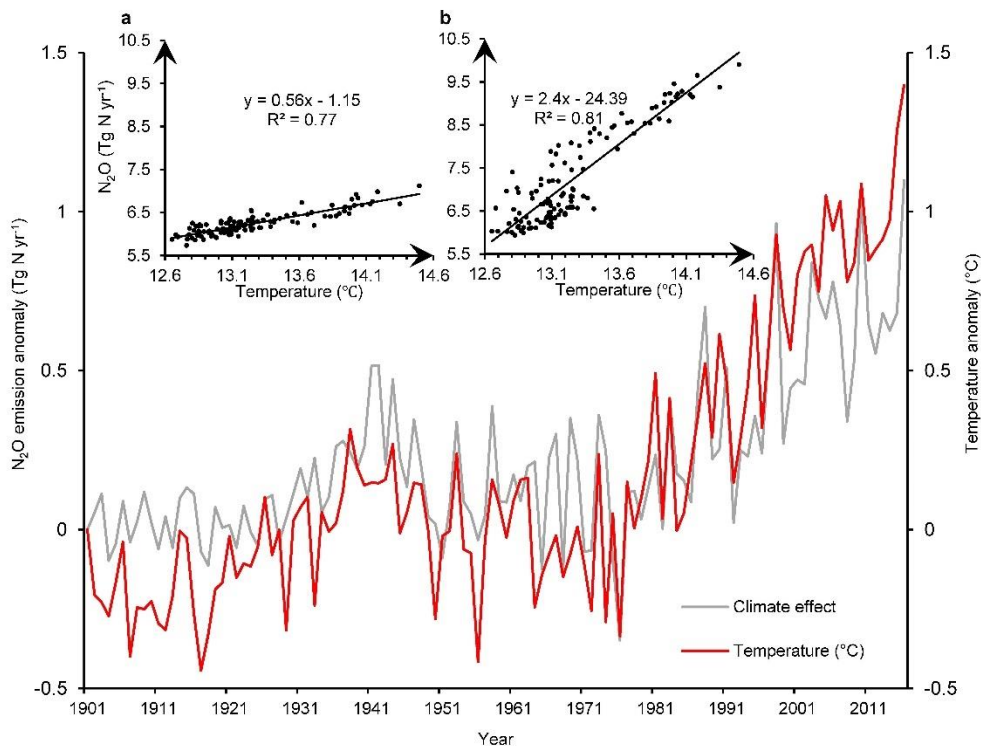


1113
 1114 **Extended Data Fig. 6 Global N₂O emissions from natural soils, inland and coastal waters**
 1115 **and due to change in climate, atmospheric CO₂ and N deposition.** **a**, Changes in global soil
 1116 N₂O fluxes due to changing CO₂ and climate. **b**, Global natural soil N₂O emissions without
 1117 consideration of land use change (e.g., deforestation) and without consideration of indirect
 1118 anthropogenic effects via global change (i.e., climate, elevated CO₂, and atmospheric N
 1119 deposition). The estimates are based on NMIP estimates during 1980–2016 including six
 1120 process-based land biosphere models. Here, we also subtracted the difference between with and
 1121 without consideration of secondary forests emissions that grow back after pasture or cropland
 1122 abandonment from natural soil emissions based on NMIP estimates. The solid lines represent the
 1123 ensemble and dashed lines show the minimum and maximum values. **c**, Global anthropogenic
 1124 N₂O emission from inland waters, estuaries, coastal zones based on models (model-based),
 1125 FAOSTAT, GAINS, and EDGAR v4.3.2 estimates. **d**, Emission due to atmospheric N deposition
 1126 (NDEP) on land based on NMIP, FAOSTAT/EDGAR v4.3.2, and GAINS/EDGAR v4.3.2.
 1127 FAOSTAT/EDGAR v4.3.2 or GAINS/EDGAR v4.3.2 means the combination of agricultural
 1128 source from FAOSTAT or GAINS with non-agricultural source from EDGAR v4.3.2. A process-
 1129 based model DLEM³⁶ and a mechanistic stochastic model^{35,51} were used to estimate N₂O
 1130 emission from inland waters and estuaries, while site-level emission rates of N₂O were upscaled
 1131 to estimate global N₂O fluxes from the global seagrass area⁶⁸.

1132
 1133

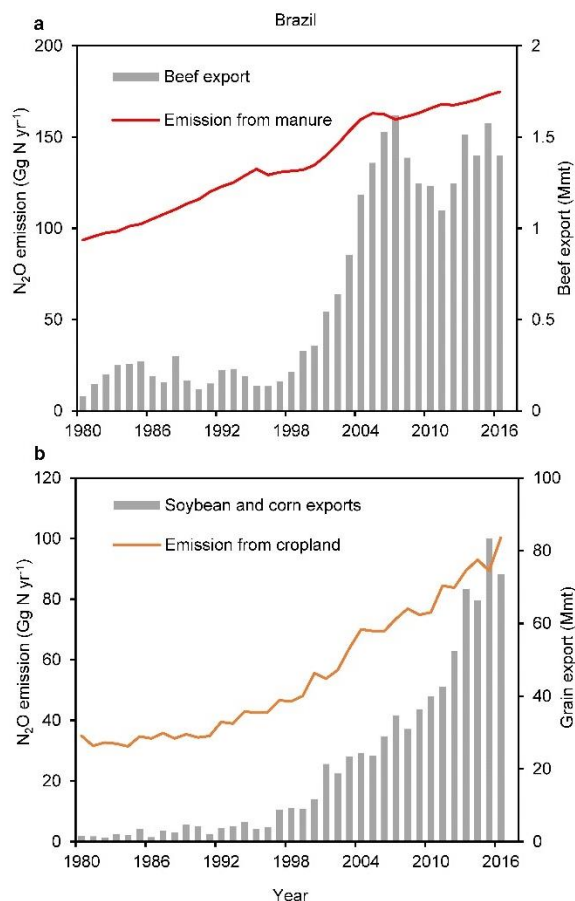


1134
 1135 **Extended Data Fig. 7 Global N₂O dynamics due to land cover changes.** The blue line
 1136 represents the mean forest N₂O reduction caused by the long-term effect of reduced mature forest
 1137 area (i.e., deforestation) and shaded areas show minimum and maximum estimates; the red line
 1138 represents the mean N₂O emission from post-deforestation pulse effect (i.e., crop/pasture N₂O
 1139 emissions from legacy N of previous forest soil, not accounting for new fertilizer N added to
 1140 these crop/pasture lands) and shaded areas show minimum and maximum estimates; the gray line
 1141 represents the mean net deforestation emission of N₂O and shaded areas show minimum and
 1142 maximum estimates.
 1143
 1144

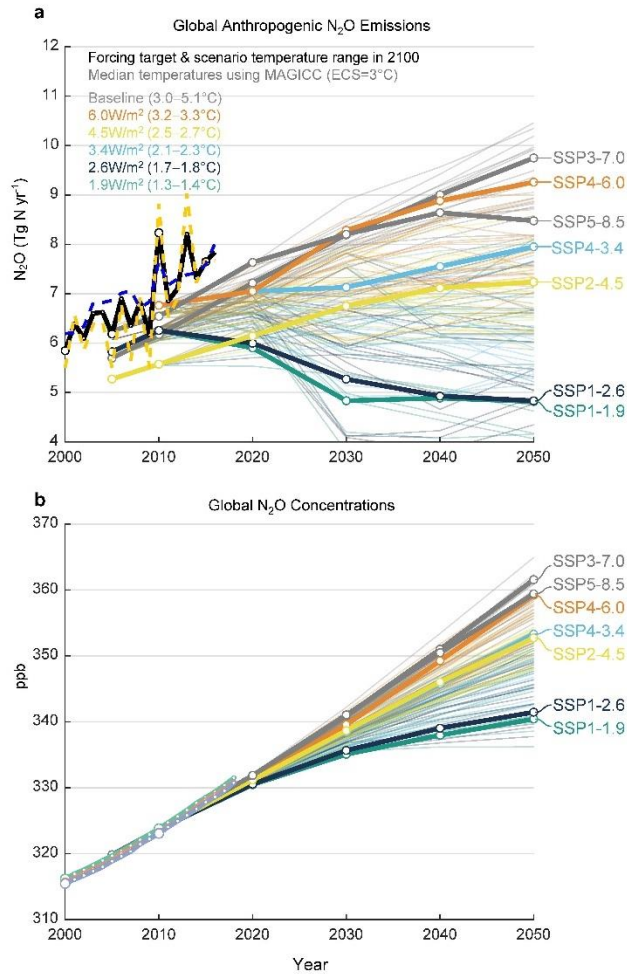


1145
 1146 **Extended Data Fig. 8 Global simulated N₂O emission anomaly due to climate effect and**
 1147 **global annual land surface temperature anomaly during 1901–2016.** Global N₂O emission
 1148 anomalies are the ensemble of six process-based land biosphere models in NMIP. The
 1149 temperature data were obtained from the CRU-NCEP v8 climate dataset
 1150 (<https://vesg.ipsl.upmc.fr>). The above left figure **a**) shows the correlation between average global
 1151 annual land surface temperature and simulated N₂O emissions (i.e., the result of SE6 experiment
 1152 in NMIP¹⁶) considering annual changes in climate but keeping all other factors (i.e., N fertilizer,
 1153 manure, NDEP, elevated CO₂, and land cover change) at the level of 1860. The above right
 1154 figure **b**) shows the correlation between average global annual land surface temperature and
 1155 simulated N₂O emissions (i.e., the result of SE1 experiment in NMIP¹⁶) considering annual
 1156 changes in all factors during 1860–2016.

1157
 1158



1159
 1160 **Extended Data Fig. 9 Direct soil emissions and agricultural product trades in Brazil.** **a**, Red
 1161 line shows the ensemble direct N_2O emissions from livestock manure based on EDGAR v4.3.2,
 1162 GAINS, and FAOSTAT, the sum of ‘manure left on pasture’ and ‘manure management’; The
 1163 gray columns show the amount of beef export by Brazil. **b**, Orange line shows the ensemble
 1164 direct N_2O emissions from croplands due to N fertilization based on NMIP and SRNM; The gray
 1165 columns show the amount of soybean and corn exports by Brazil. The data of beef and cereal
 1166 product trades were adapted from the ABIEC (beef) and FAOSTAT (soybean and corn). Mmt yr⁻¹
 1167 ¹ represents millions of metric tons per year.
 1168
 1169



1170
 1171 **Extended Data Fig. 10 An extension of Fig. 4 to provide a comparison of anthropogenic**
 1172 **N₂O emissions (a) and atmospheric N₂O concentrations (b) in the unharmonized SSPs¹⁰⁵.**
 1173 The emission and concentration data are as in Fig. 4. The unharmonized emissions from the
 1174 Integrated Assessment Models (IAMs)¹⁰⁵ show a large variation due to different input data and
 1175 model assumptions. Comparison with Fig. 4b, d illustrates the modifications to the IAM scenario
 1176 data for use in CMIP6. All baseline scenarios (SSP3-7.0 and SSP5-8.5; without climate policy
 1177 applied) are shown in gray regardless of the radiative forcing level they reach in 2100.